Nat. Hazards Earth Syst. Sci., 13, 1025–1050, 2013
www.nat-hazards-earth-syst-sci.net/13/1025/2013/
doi:10.5194/nhess-13-1025-2013

Natural Hazards and Earth System Sciences
Open Access

Integrating geologic fault data into tsunami hazard studies

R. Basili[1], **M. M. Tiberti**[1], **V. Kastelic**[2], **F. Romano**[1], **A. Piatanesi**[1], **J. Selva**[3], **and S. Lorito**[1]

[1]Istituto Nazionale di Geofisica e Vulcanologia, Via di Vigna Murata 605, 00143 Rome, Italy
[2]Istituto Nazionale di Geofisica e Vulcanologia, Via Arcivescovado 8, 67100 L'Aquila, Italy
[3]Istituto Nazionale di Geofisica e Vulcanologia, Via Donato Creti 12, 40128 Bologna, Italy

Correspondence to: R. Basili (roberto.basili@ingv.it) and M. M. Tiberti (mara.tiberti@ingv.it)

Received: 31 October 2012 – Published in Nat. Hazards Earth Syst. Sci. Discuss.: –
Revised: 31 January 2013 – Accepted: 6 February 2013 – Published: 19 April 2013

Abstract. We present the realization of a fault-source data set designed to become the starting point in regional-scale tsunami hazard studies. Our approach focuses on the parametric fault characterization in terms of geometry, kinematics, and assessment of activity rates, and includes a systematic classification in six justification levels of epistemic uncertainty related with the existence and behaviour of fault sources. We set up a case study in the central Mediterranean Sea, an area at the intersection of the European, African, and Aegean plates, characterized by a complex and debated tectonic structure and where several tsunamis occurred in the past. Using tsunami scenarios of maximum wave height due to crustal earthquakes ($M_w = 7$) and subduction earthquakes ($M_w = 7$ and $M_w = 8$), we illustrate first-order consequences of critical choices in addressing the seismogenic and tsunamigenic potentials of fault sources. Although tsunamis generated by $M_w = 8$ earthquakes predictably affect the entire basin, the impact of tsunamis generated by $M_w = 7$ earthquakes on either crustal or subduction fault sources can still be strong at many locales. Such scenarios show how the relative location/orientation of faults with respect to target coastlines coupled with bathymetric features suggest avoiding the preselection of fault sources without addressing their possible impact onto hazard analysis results.

1 Introduction

Following the destructive tsunami of the Indian Ocean in 2004, Probabilistic Tsunami Hazard Analysis (PTHA) has gained more attention than in the past. Especially in areas where empirical data are drawn from incomplete earthquake and tsunami catalogs, it becomes a necessity to found PTHA upon modelling of the seismic source and of the tsunami propagation. Considering that earthquakes are generally the most likely sources for tsunami generation, PTHA often borrows concepts and methods (Geist and Parsons, 2006) from Probabilistic Seismic Hazard Analysis (PSHA). However, among the various additional difficulties that arise when performing PTHA as opposed to PSHA, there exists an instance of specific difficulty related with the potentially tsunamigenic offshore faults that are generally poorly constrained.

To date, most PTHA studies focused on subduction zones because, as experience shows, they are the sources of earthquakes that can generate the biggest tsunamis. Various levels of detail were applied to describe the subduction geometry, often in consideration of the distance from the target coasts or other technical factors (Annaka et al., 2007; Burbidge et al., 2008; González et al., 2009; Power et al., 2012). Burbidge et al. (2008) also took into account fault sources other than megathrusts associated with subduction zones and used criteria based on the expected potential tsunami threat to preselect the fault sources to be included in the analysis. Some PTHA studies mainly relied on earthquake catalogs to delineate broad area sources (Mitsoudis et al., 2012; Sørensen et al., 2012) or gridded seismicity (Grezio et al., 2012). Recurrence time or frequency of earthquake sources is often based on the Gutenberg–Richter power law (Power et al., 2007; Burbidge et al., 2008; Power et al., 2012; Grezio et al., 2012; Sørensen et al., 2012) or the characteristic earthquake model (Annaka et al., 2007; González et al., 2009) or both (Geist and Parsons, 2006).

Mapping of active offshore faults may highlight the presence of potentially tsunamigenic sources that can be critical in areas where seismic catalogs are deficient or where the earthquake recurrence interval is very long compared with

the length of the catalog or where fault activity is episodic (long periods of silence interrupted by burst of activity). However, fault identification, characterization, and evaluation of the tsunamigenic potential are particularly challenging because (1) most of the necessary data comes from infrequent geologic studies in the offshore and (2) in tsunami studies there is a need to investigate very large areas. These are the main two reasons for geologic fault data incompleteness.

Although the use of fault sources is likely one of the most suitable ways to perform region-wide PTHA, the identified and characterized fault sources may have significantly different levels of epistemic uncertainty at the moment of a PTHA effort. The first step in addressing these epistemic uncertainties requires defining the level of knowledge on the existence of the proposed fault sources and characterizing them in a hierarchical framework. Subsequently, epistemic uncertainties will mainly involve the type and rate of earthquake production of those fault sources. Finally, an evaluation of the completeness level of the fault data set is critical. In effective PTHA studies, potential gaps in fault knowledge should be compensated by area sources or smoothing kernels with diffuse and/or background seismicity. To deal with these uncertainties, different methodologies may be adopted, such as logic trees (e.g. Geist and Parsons, 2006; Annaka et al., 2007), Bayesian inference (e.g. Grezio et al., 2010; Selva et al., 2010), or even expert elicitation (e.g. Neri et al., 2008; Selva et al., 2012). However, a specific focus is necessary on detailing the gamut of choices that PTHA practice will face from mapping and parameterizing fault sources to estimating earthquake recurrence times. All these issues should be addressed before running tsunami simulations for calculating wave propagation and/or run-up, that is to say, in preparing the fault database.

To explore the initial steps that need to be taken for integrating geologic fault data in region-wide PTHA, we develop a case study in the central Mediterranean Sea, an area located at the intersection between the European, African, and Aegean plates, and known for having been historically affected by tsunamis generated by crustal and subduction earthquake sources of very variable types and dimensions (Fig. 1). Historical tsunamis in the central Mediterranean Sea have caused significant effects and damage even when generated by moderate earthquakes (NGDC/WDS Global Historical Tsunami Database). This might have been caused by a combination of factors, including the small size of the basin compared with the number of potential sources at short distance from coastlines. Historical earthquake catalogs in the Mediterranean area are the most accurate and complete among those that span several centuries; however, offshore seismicity is not necessarily well captured in those catalogs. On the one hand, an approach that relies mostly on known seismicity may fail in identifying and characterizing many potential tsunamigenic sources. On the other hand, there is no apparent way of determining the sufficient number of fault sources in an input data set for performing PTHA, and the evaluation of activity rates may necessarily rely on average long-term geologic fault behaviour.

Our study presents the design and realization of a PTHA-oriented input data set of fault sources that may become the starting point for a region-wide hazard study. We focus on the classification of epistemic uncertainties related with the existence and behaviour (e.g. temporal recurrence model, size distribution) of the fault sources. As an example, we present a possible formalization of epistemic uncertainty treatment in a logic tree for which we illustrate one pattern of choices being made to derive activity rates from a consistent recurrence model that exploits the geologic fault properties. However, notice that a full characterization of fault sources also should include geometric and kinematic parameterization whose epistemic uncertainties are not analysed here, since they deserve further dedicated sensitivity studies. Accordingly, we do not investigate further epistemic uncertainties like those related to modelling of seafloor displacement, tsunami generation, and propagation (e.g. Geist, 2009; Løvholt et al., 2012a). We limit ourselves to roughly assess the overall tsunamigenic potential associated to the faults here analysed. We accomplish this task by running several sample scenarios based on quite standard techniques and then we analyse the maximum wave Heights ($H_{\max}$) generated along the coasts of the central Mediterranean Sea. Although a comprehensive PTHA study is beyond the purpose of this paper, combining a logic-tree approach or a Bayesian approach with our analyses may represent the basis to evaluate the impact that epistemic uncertainties on fault sources may have onto the hazard calculations.

2 Method and rationale

The compilation of an input data set for PTHA is a rather long process that includes identification, mapping, and characterization of fault sources, and requires the systematic inspection of many different data types. When tackling a PTHA of a region, at the end of the compilation process the resulting data set can include fault sources of any of the following three different types.

Fault Type 1: coastal and offshore structures that are fully parameterized and their epistemic uncertainty addressed. In our data set, we classify these faults into two categories: crustal fault sources and subduction fault sources. The main reasons for keeping these two categories separated for tsunami hazard studies are summarized in Table 1.

Fault Type 2: known offshore structures, or possible continuation of known onshore faults, whose capability of releasing earthquakes of significant magnitude is unknown or not yet investigated. Fault sources of this type can also be alternative solutions to fault sources of Type 1. These fault sources can also be parameterized.

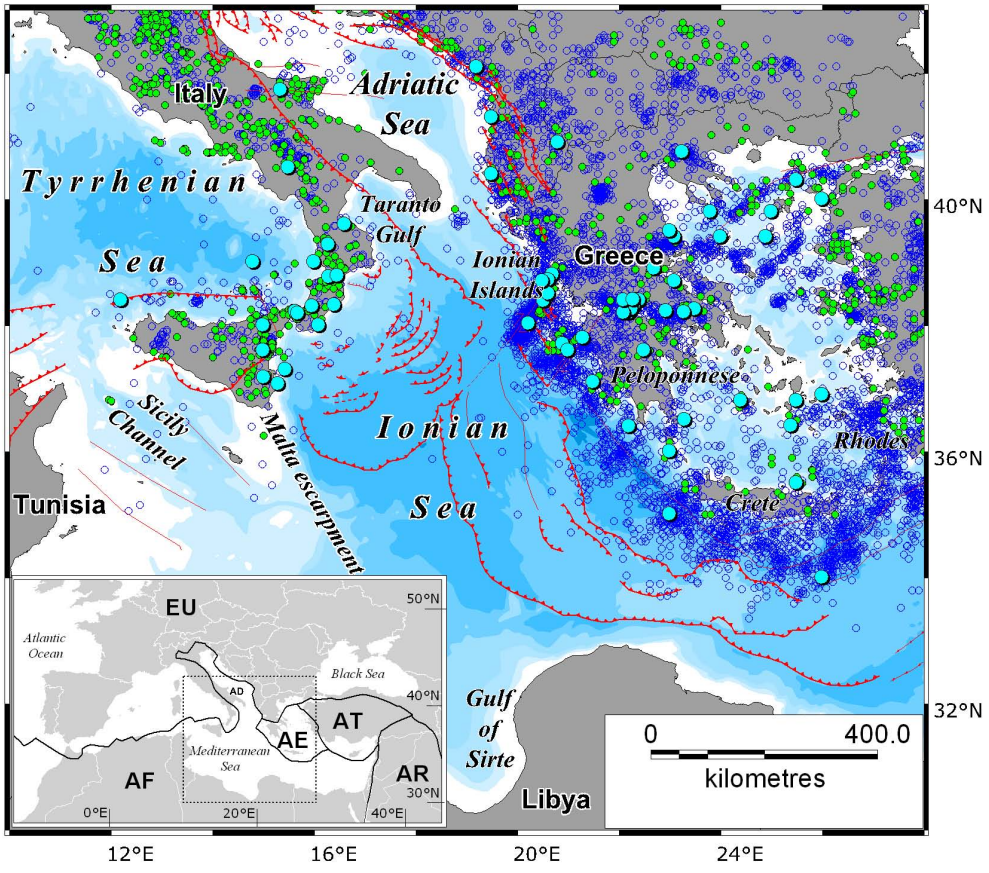

Fig. 1. Map of the study area showing the main tectonic structures (red lines represent faults; saw-toothed red lines represent thrust faults), seismicity from SHEEC (green solid circles; data from Stucchi et al., 2012) and EMEC (blue open circles; data from Grünthal and Wahlström, 2012), and tsunami sources (light-blue large solid circles) from NGDC/WDS Global Historical Tsunami Database. Inset shows the general tectonic setting of the central Mediterranean Sea. Legend for tectonic plates: EU, Eurasian; AF, African; AE, Aegean; AT, Anatolian; AR, Arabian. Notice the Adria Microplate (AD), a promontory of the African Plate, which acts as an indenter in between the Apennines to the west, the Alps to the north, and the Albanides–Dinarides to the east, all facing the Adriatic Sea.

Table 1. Summary of modelling approaches for crustal and subduction sources.

	Crustal fault sources	Subduction fault sources
3-D geometry	Simple planar dipping surface (constant dip or dip direction) can be used.	Need to use complex dipping surface (dip and dip direction vary with depth).
Mechanical properties	Uniform half space, constant rigidity, and constant stress drop are viable simplifications.	3-D heterogeneous medium. Trade off between rigidity and stress drop should be considered (Bilek and Lay, 1999).
Scaling laws	Various relationships can be applied depending on faulting type and/or tectonic setting and crustal properties (e.g. stable continental region vs. active margin).	Requires application of fault scaling laws specifically derived for subduction earthquakes and distinction between interface and intraplate faulting (e.g. Strasser et al., 2010).
Seafloor displacement	Can be effectively obtained from modelling of fault dislocation in a uniform half space (e.g. Okada, 1985).	Dislocation modelling that better takes into consideration the geometrical and mechanical properties is desirable (e.g. finite element modelling).
Near field/far field	Small crustal faults can be important if they are close to target.	Subduction zones are important even if they are very distant from target.

Fault Type 3: structures located in areas with known or possible seismic/tectonic activity, but where fault identification and mapping has not yet been carried out. This condition may occur for different reasons, e.g. scarcity of geophysical/geological data at the scale of interest, and/or complex fault systems with many structures whose relative importance is difficult to discriminate. These potential sources can be described by area sources and their parameters treated stochastically.

Dependencies among fault sources of different types have to be identified, and cases of sources that are mutually exclusive clearly labelled to avoid double counting. The relative importance that each source type has in the hazard assessment has to be evaluated by the hazard modellers.

The making of such data sets relies almost exclusively on critical review of published geologic and tectonic data about coastal and offshore structures. Differently from onland studies of active faulting, the coastal and offshore structures are less accessible and, therefore, more difficult to be mapped. Submarine paleoseismological investigations are rare because they are mainly conducted through high-resolution seismic profiles and well data. Geometry and kinematics of faults at depth mainly rely on hydrocarbon exploration data, if available. Seismicity data can help with fault characterization in the coastal zone, but they are usually not accurate enough in the offshore unless highly expensive OBS (ocean bottom seismometer) network experiments are carried out. In onshore PSHA, recurrence models based on detailed knowledge of segment boundaries are often used (e.g. Petersen et al., 2008; Stirling et al., 2012). If this could be an option in onshore studies, the above illustrated circumstances suggest that when most faults are located offshore, as it is the case of tsunami hazard studies, the extensive use of fault segmentation models cannot be a viable option. Although only a small set of parameters is commonly used to characterize fault sources in PSHA (Haller and Basili, 2011), all these parameters are uncertain, their uncertainty has to be characterized, and its impact onto the hazard estimates be evaluated. All faults included into such data sets are assumed to be able to release earthquakes equal or larger than a minimum magnitude that usually reflects an engineering requirement or a dimensional limit (in either length or width or displacement) for the identification of faults.

The fundamental epistemic uncertainty to be assessed in the characterization of fault sources is the fault activity or, more importantly, its "existence", which involves criteria that provide an indication for the potential of future earthquake occurrence. Such criteria include spatial or causal association with past earthquakes, evidence for geologically recent displacement, structural association with other active faults, orientation relative to the regional stress regime, and other considerations (see Budnitz et al., 1997, Vol. 1, §4.3). Based on concepts of propositional knowledge, the list of declarations in the left-hand column of Table 2 provides a way for rating the relative usefulness of these criteria. The capability of a fault to release earthquakes is rated on the basis of how this property is known, i.e. the justification level for taking the fault into consideration. Each successive proposition in this list represents a lower level of knowledge (higher epistemic uncertainty).

In all cases, it is implicitly assumed that the earthquake considered in each proposition has a magnitude equal to or larger than the minimum value that was adopted for including a fault source in the data set, not the minor seismicity. In cases #1–3 the lower level of knowledge of the fault is dictated by the higher level of inference needed in a study to associate an event (the earthquake) that is progressively more distant in time to its cause (the causative fault). Case #4 represents a higher level of inference because it depends on indirectly acquired knowledge based on an association between different geological structures. The last two cases involve all geological criteria used to classify active faults based on their long-term activity, based, for example, on the displacement of geological markers (case #5) or based on how favourably their strike and dip are with respect to the present stress regime (case #6).

In order to assess the epistemic uncertainty about the existence of tsunamigenic fault sources, it is necessary to opportunely adapt the criteria used in the propositions for potential of future earthquake occurrence to take into account empirical data or prospective analysis about tsunamis. The list of propositions in the right-hand column of Table 2 could then be used.

The statements of cases #4, #5, and #6 require that the fault be located on the coast or offshore or is somehow capable of significantly displacing the sea bottom during an earthquake.

Empirical data to address cases #1–4 for justifying the existence of tsunamigenic fault sources are usually rarer and more difficult to interpret than for seismogenic fault sources. In the absence or scarcity of empirical data, any fault located near the coast or offshore, can be thought of having a certain tsunamigenic potential because it can be considered capable of displacing the seafloor. In addition to the initial seafloor displacement, some aspects of tsunamigenic potential can be better highlighted by numerical tsunami simulations that will show the wave propagation properties and the bathymetric effects in the basin domain under study.

In the following sections we present a fault-source data set compiled for the central Mediterranean Sea using the classifications described above for addressing the justification level of the faults. The available empirical data on seismogenic and tsunamigenic properties of fault sources are discussed. The natural variability about fault parameters (aleatory uncertainty) is given in ranges of minimum and maximum values.

To illustrate the possible uses of the presented epistemic uncertainties, we show an example of how they can be incorporated in a logic tree (Fig. 2), which includes alternative model options from fault identification to the determination of activity rates. Depending on the hazard analysis

Table 2. Classification scheme for the justification levels of seismogenic (left) and tsunamigenic (right) behaviour of fault sources.

Just. level	Propositions for seismogenic behaviour	Propositions for tsunamigenic behaviour
	One knows that a fault exists because it generated …	One knows that an existing fault generated …
#1:	an earthquake known from instrumental recordings;	a tsunami known from instrumental recordings;
#2:	an earthquake known from historical accounts;	a tsunami known from historical accounts;
#3:	a pre-historical earthquake known for its paleoseismological evidence (e.g. surface rupture, seismites, liquefaction, tsunami deposits);	a pre-historical tsunami known from geological records (e.g. tsunami deposits);
#4:	no earthquake, but the fault belongs to a fault system in which at least one neighbouring fault is classified as case #1, #2 or #3;	no tsunami, but the fault belongs to a fault system in which at least one neighbouring fault is classified as case #1, #2 or #3 and is capable of displacing the seafloor;
#5:	no earthquake, but the fault belongs to a system that is thought to be active;	no tsunami, but the fault belongs to a system that is thought to be active and the fault is capable of displacing the seafloor;
#6:	no earthquake, but there is some evidence that the fault would do so.	no tsunami, but there is some evidence that the fault would do so.

to be performed, however, a logic tree can be designed very differently from the one we show here for taking into account the main elements of our study. To address the recurrence of potential tsunamigenic earthquake ruptures we adopt the Gutenberg–Richter (GR) law transformed by Kagan (2002a) into the "Pareto" distribution for scalar seismic moment. This moment–frequency distribution (MFD) is truncated at a maximum moment value and follows the moment rate conservation principle (Kagan, 2002b). The characterization of fault sources includes the minimum set of parameters that is necessary for calculating the seafloor displacement caused by a potential rupture and the ensuing tsunami. For subduction sources only, we also illustrate a nested logic tree (lower panel in Fig. 2) for treating some other fault parameters, such as the maximum seismogenic depth, long-term aseismic factor, and moment upper bound, which may strongly affect the estimation of activity rates.

For each crustal fault source included in our data set we show a sample tsunami scenario for an $M_w = 7$ earthquake; for the two subduction sources we show sample scenarios for $M_w = 7$ and $M_w = 8$ earthquakes.

3 Fault sources model

This section briefly summarizes the tectonic background of our case-study area. Following the rationale described in Sect. 2, we illustrate the parameters of the identified fault sources of Type 1 (Fig. 3, Tables 3 and 4) and their justification level classification (Fig. 4, Table A1). Fault sources are grouped according to the following four main tectonic domains: A, Hellenides Fold-and-thrust Belt; B, Hellenic Arc; C, Calabrian Arc; D, Sicily–Tunisia Graben. Groups B and C include both crustal and subduction fault sources. For what concerns the latter, we do not illustrate details of intraslab and outer-rise faulting that can be generally included in Type 3. Types 2 and 3 of crustal fault sources are briefly illustrated. In addition to these fault sources, our subsequent analysis also incorporates onshore and offshore fault sources from the DISS (Database of Individual Seismogenic Sources) (Basili et al., 2008; DISS Working Group, 2010), where available, as shown in Fig. 3. Unless otherwise noted, all seismicity information given in the following description is taken from SHEEC (SHARE European Earthquake Catalog) (Stucchi et al., 2012) and EMEC (European-Mediterranean Earthquake Catalog) (Grünthal and Wahlström, 2012) catalogs. In subsequent text and in all relevant figures and tables, each fault source is referred to by a code formed by a letter (A, B, C, and D for crustal fault groups, and S for subductions) followed by an ordinal number.

3.1 Tectonic background

The central Mediterranean Sea is tectonically dominated by the interaction of the African, Eurasian, and Aegean plates (Figs. 1 and 3). The African oceanic crust (Ionian Sea) is subducted beneath the European Plate in the Calabrian Arc and beneath the Aegean Plate in the Hellenic Arc. A promontory of continental crust of the African Plate, often referred to as the Adria Microplate, separates the northward continuation of the two subduction zones.

Although the two slabs belong to the same plate, the Calabrian and Hellenic subductions are different in terms of both geometry and behaviour. The Hellenic slab dips to the north-northeast at a shallow angle (ca. $20-30°$, e.g. Papazachos et al., 2000; Suckale et al., 2009; Gesret et al., 2011), whereas the Calabrian slab is much steeper (ca. $70-80°$,

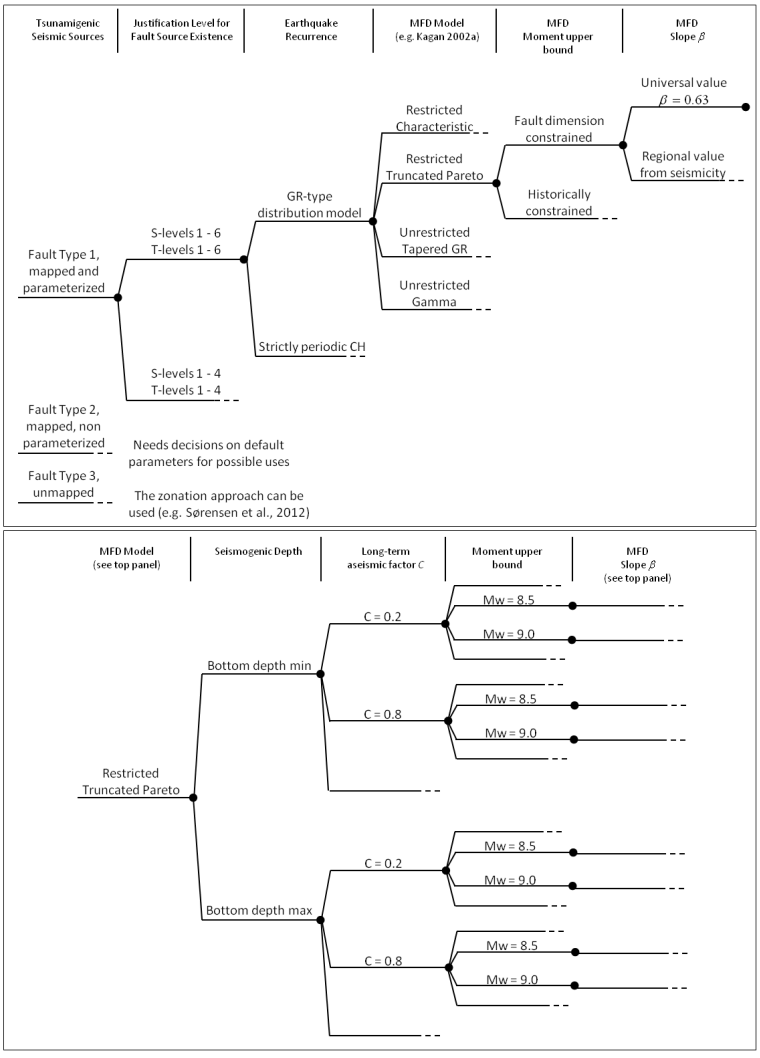

Fig. 2. Example of a simplified logic tree for fault source parameters (Fault Type 1); weights are not assigned. The upper panel is dedicated to crustal fault sources. The lower panel shows a nested branch emanating from the MFD model node for treating additional epistemic uncertainties in the recurrence rate estimation for subduction sources. Notice that some of these quantities may also, or even preferably, be treated as distributions rather than branches (e.g. moment upper bound). Different model strategies may also apply to fault sources (Fault Type 1) with lower justification level and/or for fault sources characterized by different sets of parameters (Fault Types 2 and 3).

e.g. Chiarabba et al., 2008) and dips to the northwest. Convergence rates are in the order of 35 mm yr^{-1} in the Hellenic Arc (Reilinger et al., 2006) and 1–5 mm yr^{-1} in the Calabrian Arc (D'Agostino and Selvaggi, 2004; Devoti et al., 2008; Howe and Bird, 2010; Serpelloni et al., 2010; D'Agostino et al., 2011). Wide and thick accretionary wedges developed in both zones as a consequence of the subduction processes thereby deforming the thick sediment cover accumulated over time onto the Ionian crust. Away from the subduction of the Ionian oceanic crust, the collision of continental crust is active along the coast of northern Greece and Albania, in Sicily, and in the Taranto Gulf. Intracontinental deformation occurs in the Sicily Channel and carries on toward the Gulf of Sirte (Corti et al., 2006; Serpelloni et al., 2007).

3.2 Group A: Hellenides Fold-and-thrust Belt

3.2.1 Crustal fault sources (Type 1)

The Hellenides Fold-and-thrust Belt is the result of collision between the continental crust of the Apulia domain and the Eurasian plate (Kokinou et al., 2005; Shaw and Jackson, 2010; Royden and Papanikolaou, 2011).

Six main fault sources located in the coastal and offshore zones of the Hellenides Fold-and-thrust Belt are included in our data set [A1–A6]. They have a landward (NE) dip of about 30°. A1 and A6 reach a maximum depth of 15–20 km as can be inferred from seismic lines (Velaj, 2001; Finetti and Del Ben, 2005a). All the other sources are assumed to be located within the first 10–12 km of the crust, based on

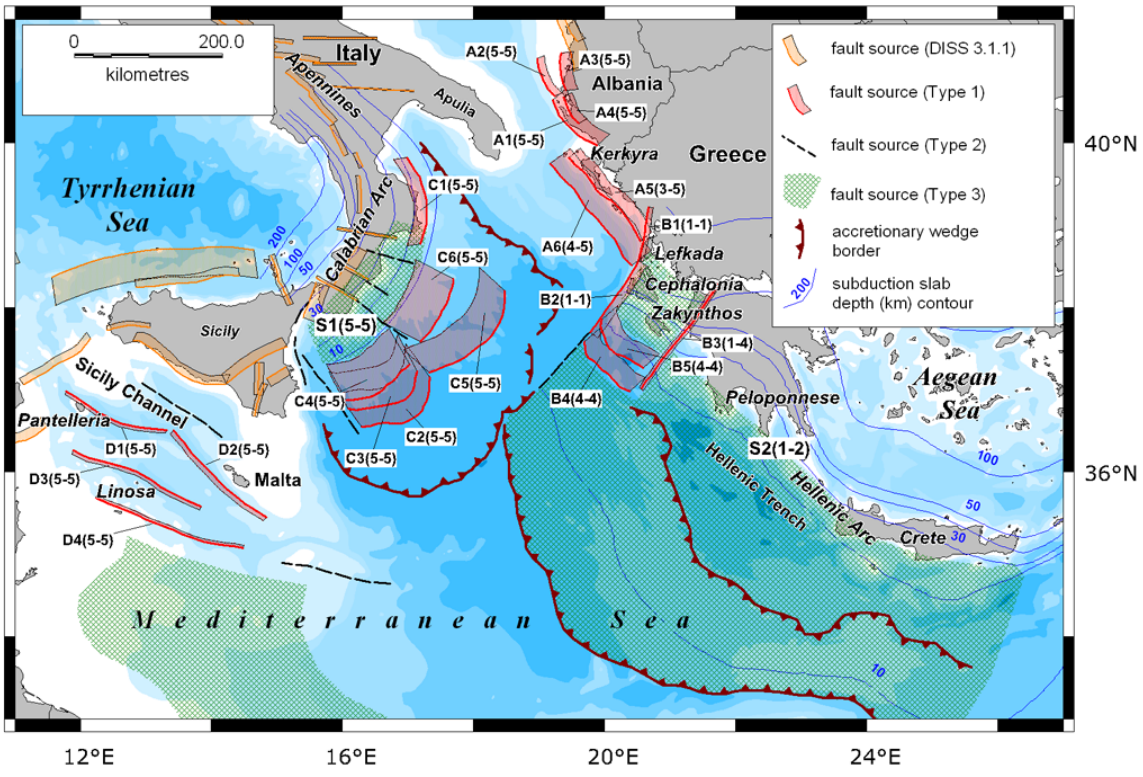

Fig. 3. Map of the fault sources in the study area. The representation of parameterized crustal fault sources (Table 3) includes the vertical projection of the fault dipping surface. Subduction slabs are shown by depth contours (for parameters see Table 4). Legend of fault identifiers (ID): A, Hellenides Fold-and-thrust Belt; B, Hellenic Arc; C, Calabrian Arc; D, Sicily–Tunisia Graben. Justification levels are shown in parenthesis as: S#-T# (see Table A1 for detailed information about the justification levels).

general considerations on the depth of the regional detachment. Slip rate values are equally partitioned to account for the 5–10 mm yr^{-1} of local convergence between the Apulia and Hellenides domains (Hollenstein et al., 2008), also considering onshore fault sources not presented here. The available focal mechanisms indicate dominant reverse faulting with SW–NE horizontal P-axes (Papazachos et al., 1999; Louvari et al., 2001); strike-slip events are also present, possibly activating tear faults (Vannucci et al., 2004; European-Mediterranean RCMT catalog by Pondrelli et al., 2006, 2007, 2011). The largest earthquakes of this area occurred in 1278, 1732 and 1786 near Kerkyra Island with estimated magnitudes of about 6.5–6.6. The largest earthquakes of the instrumental era occurred to the SE of Kerkyra Island on 5 November 1960, $M = 5.7$, on a strike-slip fault (Papadopoulos et al., 1986), and on 29 June 2007, $M = 5.6$.

3.3 Group B: Hellenic Arc

3.3.1 Subduction fault source (Type 1)

In the Hellenic Arc, the oceanic crust of the African Plate is subducted beneath the Aegean Plate. The subduction system [S2] develops along a 1000-km-long arc stretching NW–SE from Cephalonia to Crete (West Hellenic Arc) and SW–NE

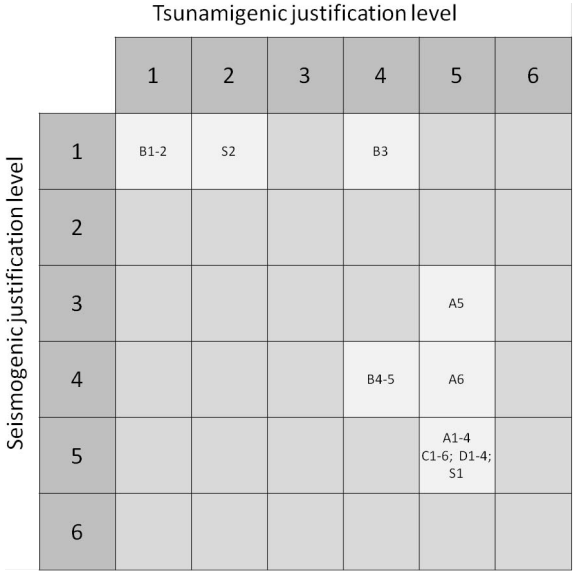

Fig. 4. Matrix for classifying the combined justification levels for the existence of fault sources in terms of both seismogenic and tsunamigenic evidences (data for this classification reported in Table A1).

Table 3. Parameters of crustal fault sources (see Fig. 3 for location).

ID	Name	Type[a]	Strike	Dip	Rake	Length	Width	Depth	Slip Rate	Moment Rate	Moment Upper Bound[b] $\times 10^{20}$ Nm			Moment Magnitude[c]		
			deg			km			mm yr^{-1}	$\times 10^{16}$ Nm yr^{-1}	Min	Avg	Max	Min	Avg	Max
A1	Sazani	DS-R	290–340	25–40	80–100	87	28	1–15	0.5–1.5	6.2	0.33	0.89	3.16	6.9	7.2	7.6
A2	Albania offshore	DS-R	300–350	20–40	80–100	57	11	2–7	0.5–1.5	1.7	0.01	0.03	0.11	6.0	6.3	6.6
A3	Seman Coastal	DS-R	330–350	20–40	80–100	52	18	1–9	0.15–1	1.1	0.07	0.18	0.64	6.5	6.8	7.1
A4	Vlora	DS-R	340–360	30–45	80–100	41	15	1–10	0.15–1.5	0.9	0.04	0.10	0.36	6.3	6.6	7.0
A5	Kerkyra	DS-R	280–350	20–40	80–100	149	22	2–12	1–2	14.2	0.15	0.41	1.47	6.7	7.0	7.4
A6	Kerkyra offshore	DS-R	280–350	20–40	80–100	176	38	3–20	1–2	28.4	1.13	3.03	10.75	7.3	7.6	8.0
B1	Lefkada	SS	5–15	60–80	160–180	74	18	3–20	4–8	23.0	0.20	0.63	1.51	6.8	7.1	7.4
B2	Cephalonia	SS	10–50	50–70	140–180	117	25	4–25	5–20	87.2	0.41	1.26	3.02	7.0	7.3	7.6
B3	Achaia	SS	200–250	70–90	140–180	176	21	5–25	2–10	48.6	0.75	2.33	5.60	7.2	7.5	7.8
B4	Mediterranean North	DS-R	300–360	15–35	80–100	96	31	5–16	1–5	19.8	0.51	1.37	4.85	7.1	7.4	7.7
B5	Zakinthos offshore	DS-R	290–360	15–40	80–100	95	33	5–17	1–5	20.7	0.62	1.67	5.93	7.1	7.4	7.8
C1	Crotone–Rossano	DS-R	145–205	20–40	80–100	124	20	3–12	0.1–1	2.4	0.10	0.28	1.00	6.6	6.9	7.3
C2	Calabria offshore SE	DS-R	180–280	5–20	80–100	135	58	4–12	0.5–1.3	18.8	2.26	6.10	21.63	7.5	7.8	8.2
C3	Calabria offshore S	DS-R	170–280	5–20	80–100	122	58	4–12	0.5–1.3	17.0	1.77	4.75	16.86	7.4	7.7	8.1
C4	Calabria offshore SW	DS-R	180–280	5–20	80–100	103	58	4–12	0.5–1.3	14.3	1.15	3.11	11.02	7.3	7.6	8.0
C5	Calabria offshore NE	DS-R	170–260	10–20	80–100	164	49	4–15	0.8-2	29.8	2.64	7.10	25.20	7.5	7.8	8.2
C6	Calabria offshore NW	DS-R	180–250	10–40	80–100	98	62	3–20	0.8–2	23.1	1.01	2.73	9.68	7.3	7.6	7.9
D1	PantelleriaN	Mixed	90–120	50–70	190–240	150	10	4–12	0.2–0.5	1.4	0.01	0.03	0.09	5.8	6.2	6.6
D2	MaltaN	Mixed	120–140	50–75	190–240	175	14	3–15	0.2–0.5	2.3	0.03	0.12	0.39	6.2	6.6	7.0
D3	LinosaN	Mixed	110–130	50–70	190–240	193	11	4–13	0.2–0.5	2.0	0.01	0.04	0.14	5.9	6.4	6.7
D4	LampedusaN	Mixed	275–300	60–80	190–230	216	11	3–13	0.3–0.8	3.5	0.01	0.05	0.15	5.9	6.4	6.7

[a] Type of faulting as used in Leonard (2010): DS = dip slip; R = reverse; SS = strike slip; Mixed = combination of normal DS, SS, and SCR.
[b] Minimum, average, and maximum values obtained from Leonard's (2010) scaling laws considering uncertainties and faulting types.
[c] Moment magnitude obtained by converting seismic moment using the relationship by Kanamori and Brodsky (2004).

Table 4. Parameters of subduction sources (see Fig. 3 for location).

ID	Name	Max conv. rate mm yr^{-1}	Azimuth CW from North deg	Dip deg	Dip direction	Depth to top km	Depth to bottom km	Length km	Width km	Moment rate $\times 10^{16}$ Nm yr^{-1} Min	Moment rate $\times 10^{16}$ Nm yr^{-1} Max
S1	Calabrian Arc	1–5	306	20	NNW	10	40–50	~ 300	88–117	47	253
S2	Hellenic Arc	35	35	30	NNE	15	40–50	~ 1000	50–70	1050	5880

from east of Crete to Rhodes (East Hellenic Arc). The western lateral termination, in the Ionian Islands, is characterized by a 100-km-wide dextral shear zone, which accommodates the different styles and rates of deformation occurring between the oceanic subduction to the east and the continental collision to the west (Feng et al., 2010; Shaw and Jackson, 2010). The eastern part of the arc is characterized by oblique contraction.

The African oceanic crust in the central Mediterranean is mostly covered by the deformed sediments of the accretionary wedge and lies as deep as 16 km (Makris and Yegorova, 2006). The slab hingeline is approximately located beneath the so-called Hellenic Trench. Further northeast, in the Peloponnese and Crete, the slab begins to dip beneath the Aegean Plate with an angle of about 20°, as imaged by seismic lines (Bohnhoff et al., 2001), receiver functions analysis (Meier et al., 2007) and results from combined seismic techniques models (Meier et al., 2004) or velocity–gravity models (Casten and Snopek, 2006; Makris and Yegorova, 2006). The slab retains a shallow angle until a depth of at least 120 km as revealed by tomographic images of P- and S-velocity variations (Papazachos and Nolet, 1997; Li et al., 2003; Suckale et al., 2009; Pearce et al., 2012). We constrained the position of the slab interface between 35 and 200 km beneath the Aegean Plate also considering the topography of the African Moho resulting from receiver function analyses of P- and S-waves (Sodoudi et al., 2006) and assuming a ~ 8 km thickness of the subducting oceanic crust as results from the work by Gesret et al. (2010) and Pearce at al. (2012). Tomographic analyses by various authors suggest the presence of the slab at very deep depth by revealing a large high velocity anomaly beneath the Aegean Sea that reaches the 660 km discontinuity (Piromallo and Morelli, 2003; Dilek and Sandvol, 2009; Suckale et al., 2009).

Seismicity distribution depicts a well developed Wadati-Benioff zone beneath the Aegean Sea to a depth of about 180 km (Hatzfeld and Martin, 1992; Benetatos et al., 2004; Bohnhoff et al., 2005; Papazachos et al., 2000; Rontogianni et al., 2011). Interface earthquakes concentrate at depth between 15 and 45 km (Taymaz et al., 1990; Shaw and Jackson, 2010; Heuret et al., 2011) and P-axes azimuth generally agree with the plate convergence direction depicted by GPS velocity vectors (McKenzie, 1978; Jackson and McKenzie, 1988; Taymaz et al., 1990; Papazachos et al., 1999; Benetatos et al., 2004).

Seismic coupling of the Hellenic subduction is generally considered weak (Becker and Meier, 2010; Reilinger et al., 2010; Rontogianni, 2010; Shaw and Jackson, 2010; Heuret et al., 2011), as moment rates and slip rates computed on the basis of seismicity account only for about 20 % of those computed on the basis of the convergence rate shown by geodetic data. However, Ganas and Parsons (2009) propose that the Hellenic subduction is fully coupled.

The Hellenic subduction is supposed to have generated one of the largest, if not the largest of all, earthquakes of the entire Mediterranean area, which occurred in 365 AD characterized by an estimated magnitude larger than 8 (Guidoboni et al., 1994; CFTI4Med by Guidoboni et al., 2007; Drakos and Stiros, 2001) and an observed coseismic uplift of up to 9 m (Pirazzoli et al., 1982).

In the Ionian Islands (Lefkada, Cephalonia, and Zakynthos) area, the subduction shows slight differences with respect to the rest of the Hellenic subduction system. Approaching this lateral termination, GPS velocities of the southward motion of the Aegean plate with respect to the African plate progressively decrease to values of about 20–25 mm yr^{-1}. Interface earthquakes concentrate within 20 km depth (Shaw and Jackson, 2010) and the calculated complete seismic coupling (Laigle et al., 2002) seems to be higher than in the rest of the Hellenic subduction (Laigle et al., 2004).

3.3.2 Crustal fault sources (Type 1): Ionian Island Transform Fault Zone

We include in this data set the main tectonic structures that characterize the northwestern lateral termination of the Hellenic Arc. Here the main structures are the NE–SW Cephalonia–Lefkada transform zone, the Achaia right-lateral strike-slip fault, and a set of NE-dipping thrust faults. Strike-slip fault sources B1–B3 are characterized by a steep dip ($> 50°$) and a maximum depth of 20–25 km, as revealed by seismic lines and seismological information on earthquake location and fault plane solutions (e.g. Louvari et al., 1999; Kokinou et al., 2005, 2006; Ganas et al., 2009; Feng et al., 2010; Shaw and Jackson, 2010). They are supposed to accommodate a horizontal velocity difference of about 30 mm yr^{-1} between the Eurasian and Aegean plates. Slip rate values can be obtained by partitioning the geodetic rates

among the fault sources [B2 and B3], considering that up to 20 mm yr^{-1} could be taken up by the Cephalonia fault source [B2] according to GPS data (Kahle et al., 1996; Hollenstein et al., 2008). These values are consistent with the long-term geological offset of 100–120 km attained by the fault in 6–8 My of activity (Royden and Papanikolau, 2011). A different partition of geodetic rates among faults inland suggests lower slip rates for the Lefkada Fault source [B1]. In between of the two sets of strike-slip fault sources, two main reverse structures [B4 and B5] affect the accretionary wedge. They are imaged in a seismic line (Kokinou et al., 2005) where they seem to reach the subduction interface at a depth of 16–17 km with a gently dipping plane. Because of lack of available data, we estimated their slip rates only on the basis of general considerations on plate convergence. Focal mechanisms from earthquakes in the area around the Ionian Islands show both strike-slip and reverse faulting (Papazachos et al., 1998; Louvari et al., 1999; Kokinou et al., 2006) with P-axes generally trending around 40° N and rotating to 80° N near Cephalonia Island (Papazachos et al., 1999).

Several $M > 6$ earthquakes hit this area since ancient times. The largest of them are the $M = 7.2$ event of 12 August 1953, in Cephalonia (Stiros et al., 1994); the 1867, $M = 7.2$, in Lixouri (Cephalonia Island); and the $M = 7.0$ transpressive event of 17 January 1983, that occurred on the southwestern part of the Cephalonia Fault source (Louvari et al., 1999). Other significant earthquakes of the instrumental era are the $M = 6.4$ strike-slip earthquake that occurred on 8 June 2008, on the Achaia Fault source (Ganas et al., 2009; Feng et al., 2010), and two events with $M = 6.5$ and with $M = 6.2$ that occurred on the southern part of the Lefkada Fault source, respectively on 22 April 1948 and on 14 August 2003 (Papadimitriou et al., 2006; Benetatos et al., 2007). The earthquakes of 1948 and 1983 also generated tsunamis (NGDC/WDS Global Historical Tsunami Database; Ambraseys and Synolakis, 2010).

3.3.3 Crustal fault sources (Type 2)

This type of fault sources can be represented by the continuation of the Cephalonia Fault source further offshore along the northwestern side of the accretionary wedge, as suggested by interpretation of seismic lines (Minelli and Faccenna, 2010; Polonia et al., 2011).

3.3.4 Crustal fault sources (Type 3)

Possible fault sources that we did not map are those in the rest of the accretionary wedge. The Hellenic subduction process generated a large accretionary wedge, usually referred to as the Mediterranean Ridge, which covers most of the Ionian oceanic crust. At places, this wedge is more than 200 km wide in the N–S direction and its southern edge reaches the African continental margin (Huguen et al., 2001; Kukowski et al., 2002; Polonia et al., 2002, Chamot-Rooke et al., 2005; Yem et al., 2011). The accretionary wedge outward growth rate was estimated at 5–20 mm yr^{-1} by Kastens (1991) and at 4 mm yr^{-1} by Kreemer and Chamot-Rooke (2004). As revealed by seismic imagery, the wedge structure is affected by large thrust faults that root at a depth of at least 8 km, (Polonia et al., 2002; Chamot-Rooke et al., 2005; Yem et al., 2011). The presence of strike-slip and back-thrust structures is also known.

There exist other possible fault sources that are commonly referred to as megasplays and are deemed to be capable of generating tsunamigenic earthquakes (Kimura et al., 2011). Megasplays are landward-dipping thrust faults that originate at the slab interface at depth and propagate updip cutting through the accretionary wedge at a steeper angle than the subducting plate. In the case of the Hellenic subduction system such faults could be located in correspondence of the Hellenic Trench (Shaw and Jackson, 2010). Shaw et al. (2008) suggested that one of such splay faults could have been the source of the 36 AD earthquake. However, since there is no clear seismic image that shows their presence in the Hellenic Arc, like in other parts of the world (e.g. Nankai Trough), we did not map these kind of possible fault sources.

3.4 Group C: Calabrian Arc

3.4.1 Subduction fault source (Type 1)

The Calabrian Arc [S1] stretches SW–NE for about 300 km between the eastern side of Sicily and the Taranto Gulf and then bends abruptly to NW and carries on as a continental collision between the Apennines and the Adria Plate. The subduction of African oceanic crust occurs only in the southernmost portion of the arc, about 200 km long.

In the Ionian Sea, the subducting plate dips at an angle of only 2–8° beneath the accretionary wedge. It becomes steeper (up to 20°) at depths greater than 10–12 km, approaching the southeastern coast of Calabria. The dip then increases again at a depth of 50 km, more or less beneath the Tyrrhenian coast. Constraints on the slab interface geometry in this area are provided essentially by seismic profiles (Finetti, 2005; Minelli and Faccenna, 2010; Polonia et al., 2011, 2012). V_p and V_s tomography reveals the presence of a high velocity anomaly beneath the Tyrrhenian Sea as deep as 600 km (Piromallo and Morelli, 2003; Chiarabba et al., 2008; Giacomuzzi et al., 2011). Seismicity distribution depicts a steep NW dipping Wadati–Benioff zone down to a maximum depth of 450 km (Chiarabba et al., 2005). The typical depth for interface earthquakes and the long-term seismic/aseismic factor are still largely undetermined for the Calabrian subduction system (Heuret et al., 2011). In the past centuries the area was struck by several $M > 6$ earthquakes; the largest of them occurred in 1638 ($M = 7$), 1783 ($M = 7$), and 1905 ($M = 6.7$). However, the possibility to associate any of them with the subduction plane is still debatable.

3.4.2 Crustal fault sources (Type 1): Calabrian accretionary wedge

The Calabrian subduction system includes a SE-verging accretionary wedge extending in the Ionian Sea for about 200 km. Recent seismic profile interpretations (Merlini et al., 2000; Van Dijk et al., 2000; Finetti, 2005; Minelli and Faccenna, 2010; Polonia et al., 2011) revealed that the accretionary wedge internal structure has two distinct lobes, the eastern lobe and western lobe, affected by large splay faults [C2–C6] deemed to be potentially seismogenic by Polonia et al. (2011, 2012). These splay faults reach the subduction plane at a depth of 15–20 km in the eastern lobe and around 12 km in the western lobe with NW dipping plane of less than 20°. Geodetic data indicate a shortening rate of $5\,\mathrm{mm\,yr^{-1}}$ across the entire accretionary wedge (Devoti et al., 2008). Slip rate values ($0.8–2\,\mathrm{mm\,yr^{-1}}$ in the eastern lobe and 0.5–$1.3\,\mathrm{mm\,yr^{-1}}$ in the western lobe) are assigned in order to account for geodetic data and are equally partitioned among the mapped structures.

To the north, the contact between Africa and Eurasia changes gradually from oceanic subduction into continental collision of the Adria domain. The main thrust is identified in our data set as fault source C1; based on seismic lines, (Van Dijk et al., 2000; Finetti, 2005; DISSWG, 2010; Capozzi et al., 2012) the fault is located between 3 and 12 km depth with a dip angle of about 30°. Having little information available about its slip rate, our estimates are based on general consideration of plate convergence.

Information about seismicity from both historical and instrumental records in this area is scarce. Several moderate earthquakes occurred off the Calabrian eastern coast, the largest of them being the $M = 5.4$ earthquake of 8 November 1983.

3.4.3 Crustal fault sources (Type 2)

The Calabrian Accretionary Wedge terminates to the SW onto the Malta Escarpment, a structure that several authors propose as being a seismogenic source (e.g. Argnani et al., 2012). Polonia et al. (2011, 2012) argue that another NW–SE shear zone, located about 70 km east of the Malta Escarpment, deforms the overlying younger deposits of the accretionary wedge and should be considered as the major tectonic feature.

Other faults that may affect the area are the seaward continuation of NNW–SSE strike-slip onshore structures that dissect the southern part of Calabria and that are imaged on seismic lines (Del Ben et al., 2008; Polonia et al., 2011; Capozzi et al., 2012). Also the thrust structures generated by continental collision in eastern Sicily could continue to the east in the Ionian Sea.

Similarly to the Hellenic Arc, also in the Calabrian Arc megasplays may play an important role in generating earthquakes and ensuing tsunamis. Clues for the presence of such structures near the Calabrian eastern coast can be found in some interpretations of seismic lines (e.g. Minelli and Faccenna, 2010; Polonia et al., 2011).

3.5 Group D: Sicily–Tunisia Graben

3.5.1 Crustal fault sources (Type 1)

The Sicily–Tunisia Graben is located in a rather unstable region of the African Plate northern continental margin, which is part of the foreland domain of the Maghrebides south-verging chain (Corti et al., 2006). Seismic reflection profiles show the presence of diffuse normal faulting associated with the formation of grabens and half grabens. The main grabens are filled with sediments with a thickness of more than 1000 m as for example, the Linosa and Pantelleria grabens (Jongsma et al., 1985; Torelli et al., 1995; Finetti and Del Ben, 2005b; Civile et al., 2010). The crust, in correspondence with the rift structure, is relatively thinned (17–25 km) with respect of the rest of the continental crust around it (Finetti and Del Ben, 2005b). The recent extensional and dextral tectonic activity is demonstrated by the displacement of Late Pliocene–Quaternary deposits and accompanied by volcanism and magmatism (Jongsma et al., 1985; Civile et al., 2010). We include in our data set [D1–D4] the main graben-bounding faults that seem to cut a significant portion of the crust (12–15 km). Geodetic data indicate NE–SW extension of $1.5\,\mathrm{mm\,yr^{-1}}$ associated with a dextral lateral component of $1.7\,\mathrm{mm\,yr^{-1}}$ across the Sicily Channel (Serpelloni et al., 2007). Slip rate values are obtained by partitioning the geodetic rates among the fault sources and considering that LinosaN [D3] has significantly greater vertical throw (Corti et al., 2006). Instrumentally recorded seismicity is rather sparse and of moderate magnitude ($M < 5$). Available focal mechanisms in the SE continuation of the fault system toward the Sirte Gulf show P-axes in agreement with the plate motion vectors, resulting in a predominant right-lateral strike-slip movement on the NW–SE fault planes, consistent with geological data (Serpelloni et al., 2007).

3.5.2 Crustal fault sources (Types 2 and 3)

The fault system in the Sicily Channel carries on southeastwardly into the Sirte Gulf and Libya (Corti et al., 2006). Seismological data (Serpelloni et al., 2007) suggest a possible strike-slip reactivation of the known NW–SE Cretaceous-Paleocene normal faults (van der Meer and Cloething, 1993; Capitanio et al., 2009).

4 Seismogenic potential

This section briefly illustrates the available data on earthquakes in the central Mediterranean Sea and their relationship with the fault sources described in Sect. 3. It also introduces the activity rate calculation and results for crustal and subduction fault sources.

4.1 Notes on earthquake empirical data

The SHEEC (years 1000–1899; Stucchi et al., 2012) and EMEC (years 1900–2006; Grünthal and Wahlström, 2012) earthquake catalogs have homogeneous determination of earthquake parameters over the entire study area. With respect to national catalogs, the pre-1900 part of the catalog relies on improved methods for possible earthquake epicenter location in the sea from macroseismic data and calibration of moment magnitude. Figure 1 shows that offshore areas are almost devoid of seismic events in the pre-instrumental era. The same is not true for on-land areas, thereby highlighting the need for a markedly different strategy in PTHA from PSHA to determine activity rates from seismicity. Fault sources located in historically "silent" zones could contribute to PTHA remarkably more than what they do in PSHA. Inclusion or exclusion of low-ranked faults based on the classification shown in Fig. 3 should be addressed by performing sensitivity tests.

4.2 Activity rates from fault sources: theoretical background

Rates of seismic activity can be estimated from tectonic moment rates of known fault sources. Moment rate $\dot{m}$ for any fault source is given by

$$\dot{m} = \mu L W \dot{D}, \quad (1)$$

where μ is rigidity, L is fault length, W is fault width, and $\dot{D}$ is slip rate. Rigidity can be derived from PREM (Preliminary Reference Earth Model) (Dziewonski and Anderson, 1981) or local data (e.g. shear wave velocity and rock density) if available. Choices of rigidity values different from PREM, however, should be considered with caution whenever conversion between seismic moment and moment magnitude is needed. Fault length, width, and slip rate are generally derived from geological and geophysical data (see Sect. 3).

The fault moment rate can be considered as a good proxy for the seismic budget of an area dominated by the activity of major faults, where the largest earthquakes occur most likely on the fault surface and smaller earthquakes may occur everywhere on and around it. The cumulative number of earthquakes equal or greater than any given size is described by the GR law. Kagan (2002a, b) transformed the original GR distribution into the Pareto distribution for scalar seismic moment that complies with the moment conservation principle. This distribution has a scale-invariant, power-law part for small and moderate earthquakes controlled by the parameter β (where β is related to the b-value of the GR distribution according to $\beta = (2/3)b$) and a moment upper bound. The parameter β is usually derived from statistics of moderate earthquakes. The moment upper bound can be derived from scaling laws that relate fault dimension to seismic moment or moment magnitude. When β, moment upper bound, and moment rate are fixed, one can thus derive the corresponding annual frequency of earthquakes.

4.3 Activity rates of crustal fault sources

The theoretical cumulative moment–frequency distributions (MFD) for the four groups of crustal fault sources of Type 1 (Fig. 5a–d), illustrated in Sect. 3 (see Fig. 2), are constructed by calculating seismic moment rate from Eq. (1) using the total length of each fault in the map, the average width, the mean slip rate, and rigidity equal to 3×10^{10} N m^{-2}. For each group the regional moment rate is obtained by summing the moment rate of each fault. No aseismic factor is considered. The scale-invariant part of the MFD uses $\beta = 0.63$ (the universal value proposed by Kagan, 2002a) and the right-hand tail uses the moment upper bound equivalent to the maximum moment of fault sources in each group as derived from Leonard's (2010) scaling laws (Table 3). This moment upper bound is derived assuming that a fault can entirely rupture either its length or width and taking the value that first saturates. Notice that fault aspect ratio is an intrinsic property of Leonard's (2010) relationships, which scale differently with magnitude for the different faulting types.

Fault sources in groups A and C are all thrusts located on active margins. These faults most often saturate the width dimension so that the moment upper bound is strongly controlled by data on fault dip and depth. Group B includes both reverse dip-slip and strike-slip faults that provide similar moment upper bound values. In strike-slip faults, the moment upper bound is generally controlled by the length dimension. In fault sources of group D, the faulting mechanism is oblique extension and the tectonic domain could be either affine to an active margin or to a stable continental region. We thus considered all types of scaling laws. For this reason, the moment upper bound has a larger uncertainty than in other fault groups.

In order to compare the so obtained MFD with actual earthquakes distributions, we convert between seismic moment (expressed in Nm) and moment magnitude using the relationship proposed by Kanamori and Brodsky (2004). Table 5 summarizes occurrences of earthquakes from the seismic catalog selected on the basis of their distance from the nearest faults. A maximum distance of 30 km was chosen as a safe criterion considering that it is about a half of the earthquake location error for historical offshore earthquakes. In the Hellenides Fold-and-thrust Belt and the Ionian Island Transform Fault Zone this comparison shows that for $M_w \geq 6$ there is a rather good agreement between recurrence intervals derived from fault sources and those that could be derived from the seismic catalog. The average earthquake frequency predicted by the tectonic rates of fault sources was significantly exceeded in the second half of the XIX century in the Hellenides Fold-and-thrust Belt and remained below average in the Ionian Island Transform Fault Zone except for the post 1950 period. The Calabrian Accretionary Wedge and the Sicily–Tunisia Graben fault sources suggest rates that can be hardly compared with seismicity. Average recurrence intervals of $M_w \geq 7$ earthquakes as predicted

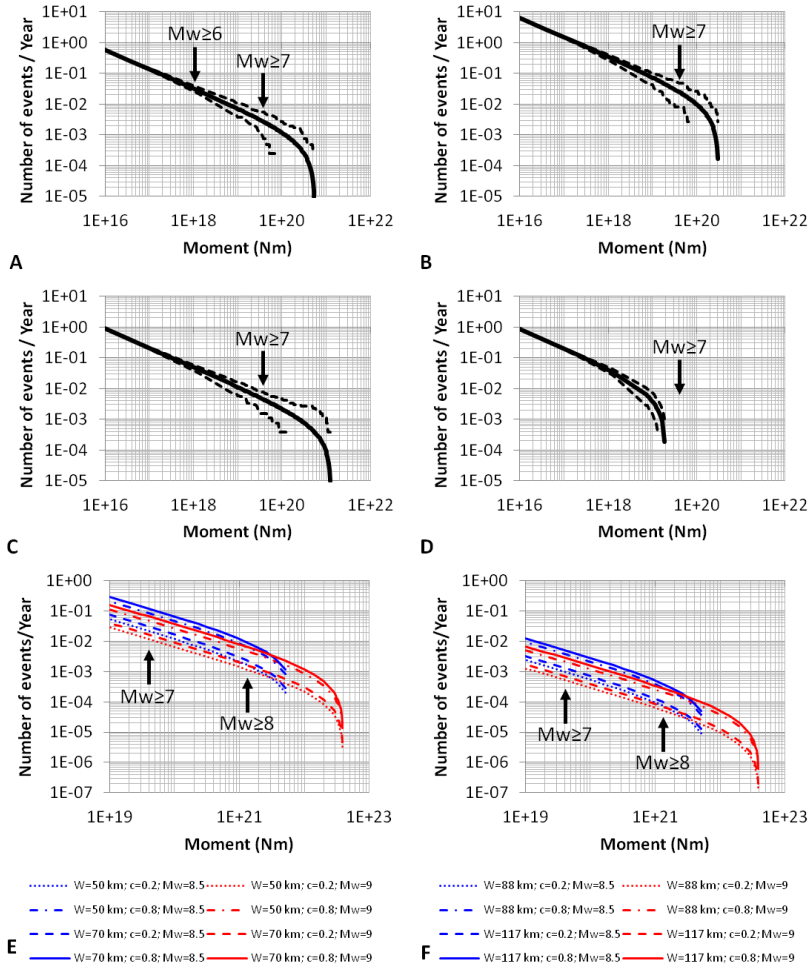

Fig. 5. (a–d) Diagrams showing the cumulative moment–frequency distribution (bold solid line) of crustal fault sources, grouped according to regional tectonic properties, based on the restrained Pareto distribution from Kagan (2002b) and constrained by the summed tectonic moment rate (Table 5): **(a)** Hellenides Fold-and-thrust Belt; **(b)** Ionian Island Transform Fault Zone; **(c)** Calabrian Accretionary Wedge; **(d)** Sicily–Tunisia Graben. The dashed lines show the cumulative minimum and maximum number of earthquakes from 100 sets of 1000 random samples according to these distributions. **(e–f)** Diagrams showing the cumulative MFD of subduction sources (slab interface) based on the restrained Pareto distribution from Kagan (2002b) and constrained by the tectonic moment rate (Table 4): **(e)** Hellenic Arc; **(f)** Calabrian Arc. W: width of slab interface constrained by seismogenic depth and average dip angle; c: long-term aseismic factor; M_{w}: magnitude upper bound.

from fault sources could easily exceed the time length of the seismic catalog in these offshore areas. However, the seemingly aseismic deformation in the accretionary wedge of the Calabrian Arc could possibly be explained by the weak rock composition (Polonia et al., 2011) and mode of tectonic loading. Rheology studies are necessary to get insights on the potential seismic behaviour of accretionary wedges. The Sicily–Tunisia Graben, instead, is an intracontinental deformation belt, and tectonic analogs onshore, such as the Rhine Graben in northwestern Europe, have been thoroughly investigated (Vanneste et al., 2013) providing insights on the capability of this type of faults to be active and seismogenic.

4.4 Activity rates of subduction sources

The theoretical MFD for the two subduction sources illustrated in Sect. 3 (see Fig. 2) are shown in Fig. 5e–f. Differently from crustal fault sources, we here consider also the epistemic uncertainty on moment upper bound, seismogenic depth, and long-term aseismic factor by showing the variability on activity rates predicted by the theoretical MFD that balances the tectonic moment rate. All MFDs are constructed using $\beta = 0.63$ and moment upper bound equivalent to a maximum moment magnitude arbitrarily set equal to 8.5 and 9. Tectonic moment rate is obtained (Table 4) using the total length of the arc where there is evidence of ongoing oceanic subduction, the mean convergence rate, average dip

Table 5. Frequency of larger earthquakes for the four groups of crustal fault sources and historically observed seismicity ($M \geq 6$) in 50-yr intervals for the last three centuries.

Fault group	Name	Total moment rate $\times 10^{16}$ Nm yr^{-1}	Moment upper bound $\times 10^{20}$ Nm	$M_w \geq 6$ in 50 yr	$M_w \geq 7$ in 50 yr	$M \geq 6$ 1700–1750	1750–1800	1800–1850	1850–1900	1900–1950	1950–2006
A	Hellenides Fold-and-thrust Belt	57.4	5.38	1–2	< 1	1	0	4	9	3	0
B	Ionian Island Transform Fault Zone	506	3.07	12–18	< 2	1	5	4	5	5	13
C	Calabrian Accretionary Wedge	119	12.7	~ 2	< 1	–	–	2	–	–	–
D	Sicily–Tunisia Graben	24.5	0.196	1–2	?	–	–	–	–	–	–

angle, and constant rigidity of 3×10^{10} N m^{-2}. The long-term aseismic factor is assumed to be 0.2 or 0.8. The seismogenic width is fixed between depth to the top of 15 km and depth to bottom of 40–50 km for the Hellenic Arc (based on Heuret et al., 2011) and depth to the top of 10 km and depth to bottom of 40–50 km for the Calabrian Arc (assumed by us, considering the lack of specific data).

The choices about the upper moment bound (difference of 0.5 in moment magnitude) generally affect the MFD for smaller earthquakes by a factor of two. The activity rate of the Calabrian Arc seems to be generally more than one order of magnitude lower than that of the Hellenic Arc. The frequency of $M_w \geq 8$ earthquakes is of 1–9 in 1000 yr in the Hellenic Arc and less than one in 2500 yr in the Calabrian Arc.

With these long recurrence intervals, the comparison with historical seismicity in subduction zones is even more challenging than that for crustal faults. The rates of larger earthquakes are very long and it is unlikely to be able to discriminate intraslab from interface earthquakes from macroseismic data alone. One possible assumption is that the very large earthquakes ($M > 8$) have occurred on the slab interface in analogy with other subduction zones. In the Hellenic Arc, however, $M = 8+$ earthquakes seem to have occurred in 365 AD and 1303, whereas in the Calabrian Arc there is no evidence of very large earthquakes in the historical record.

5 Tsunamigenic potential

This section briefly illustrates the available data on tsunamis in the central Mediterranean Sea and their relationship with the fault sources described in Sect. 3. As a demonstration of the tsunamigenic potential of the fault sources, it then introduces the calculation of tsunami scenarios and their results for a selection of crustal and subduction fault sources.

5.1 Notes on tsunami empirical data

In general, earthquakes are the most likely source of tsunamis in the world. Although other types of potential tsunamigenic geologic sources exist – such as volcano eruptions or landslides – in the central Mediterranean Sea, the NGDC/WDS Global Historical Tsunami Database lists about 18 tsunamis generated by earthquakes. This selection of events considers those tsunamis generated in the Ionian Sea in historical time, with an $M > 6$ earthquake as the most likely cause, and the highest rank for the validity of tsunami occurrence. The majority of them were generated in Greece. Eight of them were generated by earthquakes with $M > 7$, two with $M > 8$ (in 365 AD and 1303 near Crete).

However, in the Mediterranean Sea the origin of many historical tsunamis is debated. For example, among the largest tsunamis recorded in the instrumental era, the Messina Straits in 1908 was apparently caused by a normal faulting $M = 7.1$ earthquake (Pino et al., 2009 and references therein), whereas Billi et al. (2008) argued that the tsunami could have been caused by a submarine landslide.

The source of older large tsunamis is even more controversial. The 1693 tsunami was attributed to many and very different potential crustal faults and the Calabrian subduction interface (Gutscher et al., 2006) (see Table B1 for a summary) and possibly to an offshore landslide (Tinti et al., 2001), whereas Gerardi et al. (2008) exclude that the tsunami could have been generated by a landslide. However, none of the offshore fault source solutions proposed so far can explain the on-land macroseismic data on the 1693 earthquake (Visini et al., 2008, 2009).

The 365 AD earthquake of Crete was apparently generated on the Hellenic Arc and estimated to have had a moment magnitude larger than 8 by many authors. On that occasion, western Crete was apparently raised up to 9 m (Pirazzoli et al., 1982) and the tsunami produced damages at many localities of the entire Mediterranean Sea (Guidoboni et al., 1994), forming the awareness of a potentially catastrophic event, more than any other in the Mediterranean area, of a size comparable to that of mega-thrusts in the Pacific or Indian oceans.

5.2 Tsunami scenarios

Scenario-based tsunami hazard assessment has a quite long tradition (e.g. Tinti and Armigliato, 2003; Løvholt et al., 2006; Okal et al., 2006, 2011; Okal and Synolakis, 2008;

Table 6. Parameters of sample fault ruptures (see Fig. 6a) for locations.

ID	Lat[a] North	Long[a] East	Length km	Width km	Strike deg	Dip deg	Rake deg	Slip m	Top depth b.s.l. m	Mean elevation m	M_w[b]
A6	39.486	19.571	35	14	322	30	90	3	3000	1151	7
B2	38.007	20.105	49	10	35	60	160	3	4000	2624	7
B4	37.308	19.985	35	14	310	22	90	3	5000	3258	7
C4	37.049	16.571	35	14	233	12	90	3	4000	3010	7
D2	35.880	14.069	35	14	135	60	215	3	3000	941	7
S1a	37.937	16.749	35	14	218	18	90	3	10 000	1827	7
S2a	35.137	23.401	35	14	310	15	90	3	15 000	3032	7
S1b	38.019	16.616	100	45	218	18	90	9	10 000	1526	8
S2b	35.241	23.506	100	45	310	15	90	9	15 000	1729	8

[a] Lat and Long are coordinates of the top-middle point of rectangular faults. [b] Moment magnitude of sample fault source.

Lorito et al., 2008; Tiberti et al., 2008; Tinti et al., 2008; Tang et al., 2009). However, while the scenario based approach is being progressively replaced by PTHA, it can be still useful in many circumstances such as the construction of infrastructure design scenarios, or for an order-of-magnitude estimate in particularly complex tectonic settings (Løvholt et al., 2012b).

For a preliminary assessment of the relative tsunamigenic power of the fault sources, we design simplified uniform slip scenarios. A more thorough scenario design should incorporate some or all the elements summarized in Table 3. Table 6 and Fig. 6a summarize the parameters attributed to a set of sample ruptures that may occur on any of the fault sources listed in Tables 3 and 4, for which we numerically computed tsunami scenarios. These sample ruptures roughly represent $M_w = 7$ earthquakes for all crustal fault sources, and $M_w = 7$ and $M_w = 8$ earthquakes for subduction sources. Notice that these ruptures are sampled at random but taking care that they are all located entirely offshore, although their parent fault sources may be partly located inland. The parameters of these ruptures are used to initialize the built-in Okada analytical formulas (Okada, 1985, 1992) in the COMCOT (Cornell Multi-grid Coupled Tsunami Model) code (http://ceeserver.cee.cornell.edu/pll-group/comcot.htm), and then the tsunami propagation at open sea is simulated by solving the linear version of shallow water equations. The boundary conditions used are pure wave reflection at the solid boundary (coastlines) and full wave transmission at the open boundary (open sea).

The computational domain (Fig. 6b–j) for tsunami propagation has a spatial resolution of 30 arc-seconds. We use the topo/bathymetric data set SRTM30 PLUS (Shuttle Radar Topography Mission) (http://topex.ucsd.edu/WWW_html/srtm30_plus.html). For each sample fault rupture, we compute the maximum water elevation along the 50-m isobaths within the computational domain, and then we extrapolate the maximum wave heights along the coasts by using Green's Law (Synolakis, 1991).

The results of numerical simulations show that both the $M_w = 7$ and $M_w = 8$ earthquakes generated by the fault sources in our data set are potentially tsunamigenic (Fig. 6b–j). $M_w = 7$ earthquakes produce significant wave heights ($H_{max} > 0.5$ m, Fig. 6b–h) only locally, whereas $M_w = 8$ earthquakes produce significant wave heights almost everywhere in the investigated domain (Fig. 6i and j). $M_w = 8$ earthquakes, however, are likely to be generated only by the two subduction zones. The different distributions of the H_{max} for each simulated earthquake rupture point to locally different threat levels along the coasts and particularly with regards to $M_w = 7$ events. Although for relatively smaller events the tsunami exposure is significant only at local level, H_{max} smaller than 0.5 m should not be neglected because water waves of few tens of centimeters can still cause significant damages in the harbours due to resonance effects.

In principle, the tsunami waves generated by strike-slip faulting are less significant with respect to dip-slip faulting because the vertical component of seafloor displacement they cause is smaller. This consideration could somehow deceptively induce thinking that strike-slip earthquakes would not generate significant damages along the coasts. However, in some cases the bathymetry (Fig. 6a) can play an important role regarding the tsunami effects. For example, the shelf extending to the southeast of Apulia (Fig. 3) acts as a wave guide for tsunami propagation thereby focusing the energy in a relatively narrow band and enhancing the wave height that reaches the southernmost tip of Apulia. This is the well-understood continuous refraction and amplification phenomenon. Despite the slight vertical seafloor displacement caused by the strike-slip mechanism of the causative fault, the Cephalonia Fault source poses a significant threat to the coasts of southern Italy, which may be further increased by shoaling amplification (Fig. 6e). Another case of systematic amplification is caused by the extension of the continental platform in the Derna District, Libya, which seems to enhance the water height even for some cases of $M_w = 7$ earthquakes (Fig. 6c, f–h). The Malta Escarpment is another noteworthy geomorphic feature, running NNW–SSE for ca. 150 km south of Sicily, with a bathymetric step of 1000–1500 m, east side lower. This feature apparently enhances the wave height of all the tsunamis generated by fault

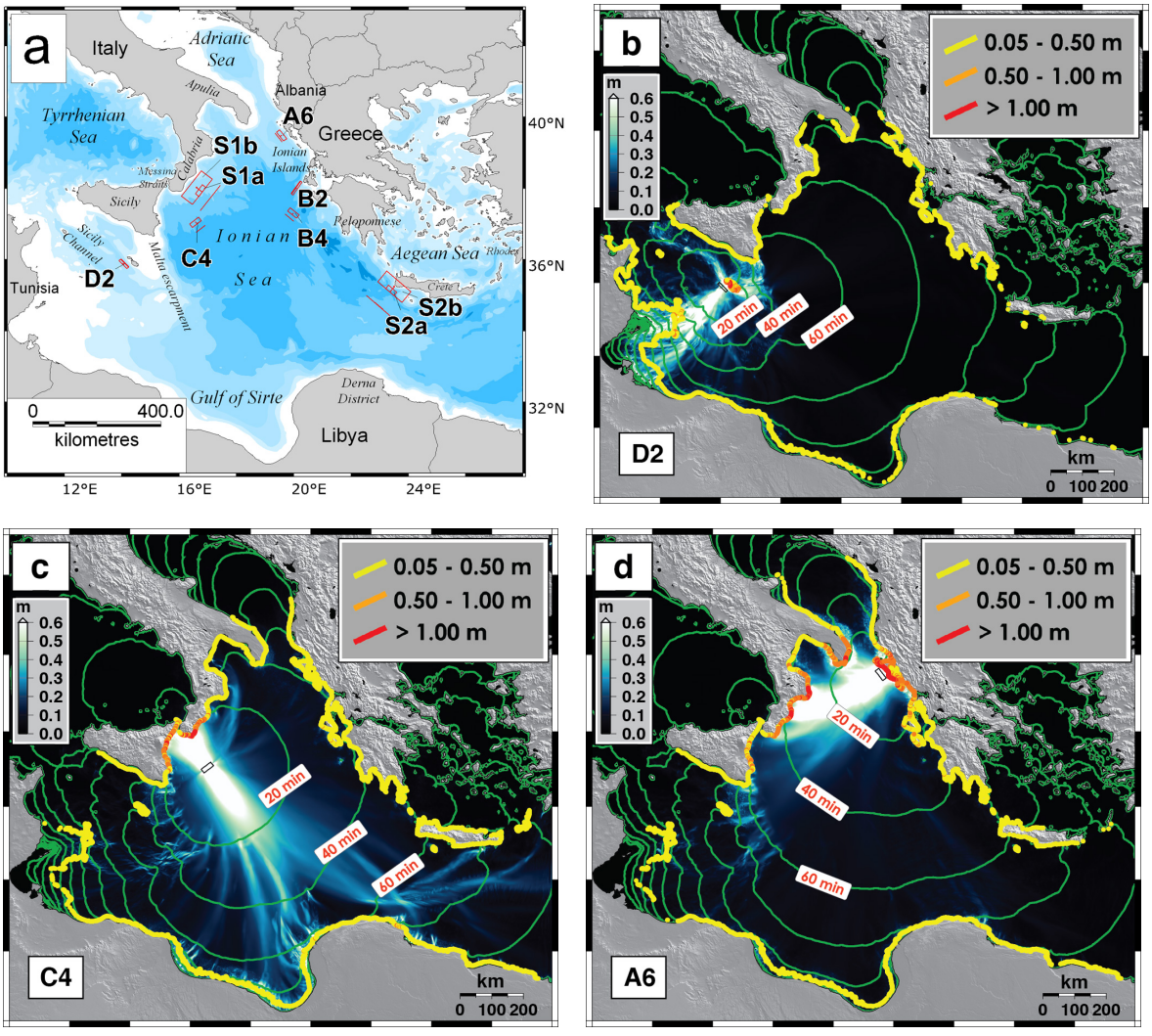

Fig. 6. Maps showing maximum wave heights (H_{max}) and tsunami travel time (green contour lines at 20 min intervals) for the exploration of the tsunamigenic potential of fault sources: **(a)** map of the individual sample ruptures (see fault parameters in Table 6); **(b)** Sicily–Tunisia Graben, crustal oblique-normal fault D2, $M_w = 7$; **(c)** Calabrian Accretionary Wedge, crustal thrust fault C4, $M_w = 7$; **(d)** Hellenides Fold-and-thrust Belt, crustal thrust fault A6, $M_w = 7$; **(e)** Ionian Island Transform Fault Zone, crustal strike-slip fault B2, $M_w = 7$; **(f)** Ionian Island Transform Fault Zone, crustal thrust fault B4, $M_w = 7$; **(g)** Calabrian Arc, subduction interface S1a, $M_w = 7$; **(h)** Hellenic Arc, subduction interface S2a, $M_w = 7$; **(i)** Calabrian Arc, subduction interface S1b, $M_w = 8$; **(j)** Hellenic Arc, subduction interface S2b, $M_w = 8$. Yellow, orange and red dots indicate the H_{max} values along the coasts lower than 0.5 m, between 0.5 and 1 m, and greater than 1 m, respectively. Black rectangles represent the surface projection of the fault sources.

sources on the eastern side of the basin, whereas it lessens the wave height of tsunamis generated by fault sources in the Sicily Channel.

6 Final remarks

Among the various epistemic uncertainties that characterize PTHA, we developed a hierarchization scheme for the justification level of existence and behaviour of potentially tsunamigenic fault sources, and showed how this rationale could be incorporated in a logic-tree approach for PTHA.

For our case study, set in the central Mediterranean Sea, we reviewed the tectonic literature to identify and map potential tsunamigenic fault sources and applied our hierarchical scheme. For crustal and subduction fault sources of Type 1 (Sect. 2) we also estimated the MFD of earthquakes they could generate and evaluated their relative tsunamigenic potential through a series of sample tsunami scenarios. Although we did not calculate tsunami hazard curves in this study, several considerations worth of notice can be drawn by inspecting the wave field and H_{max} attained at target coastlines.

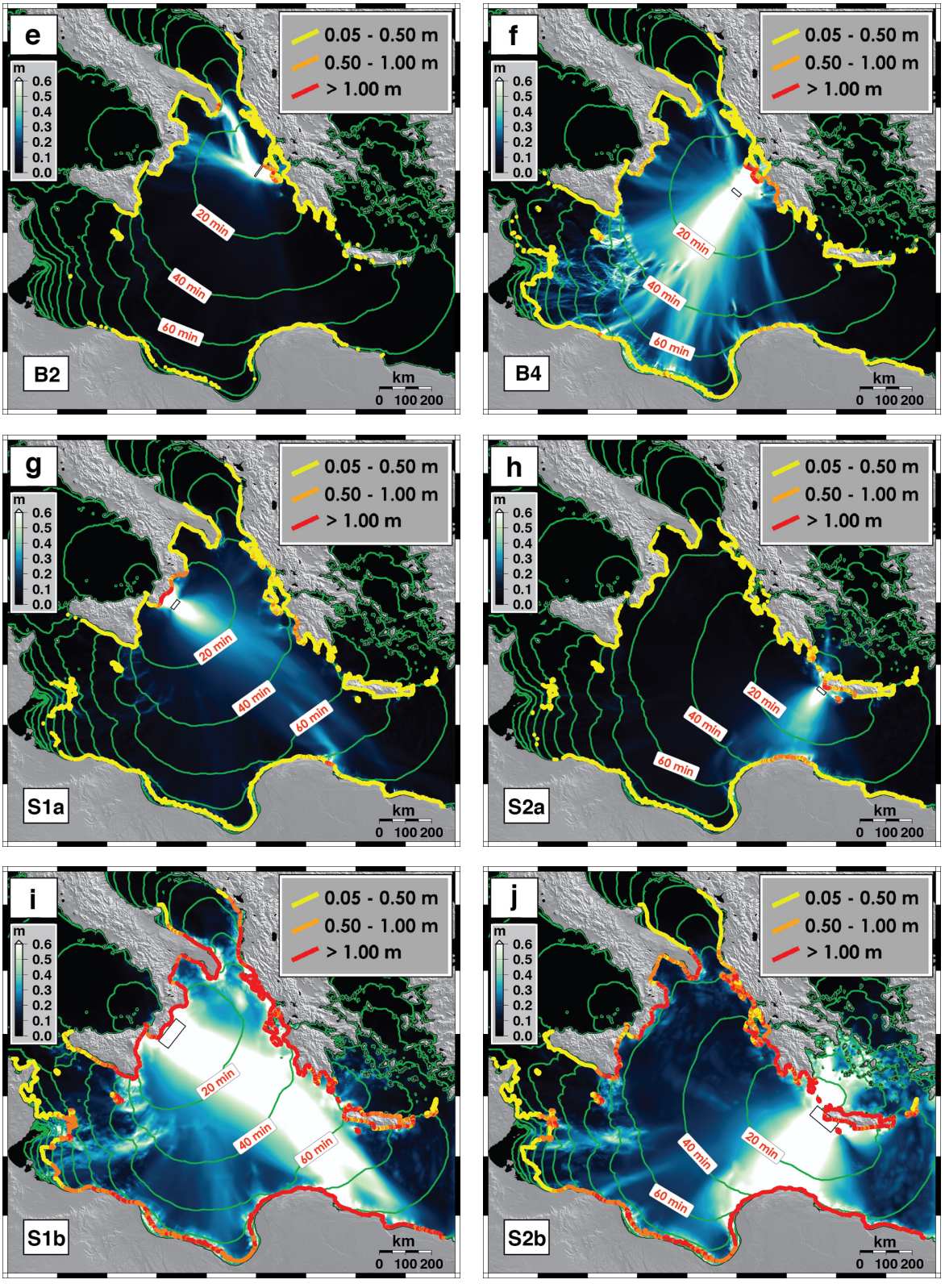

Fig. 6. Continued.

On the one hand, an $M_w = 7$ earthquake rupture in the Hellenides Fold-and-thrust Belt (fault group A) produces a pattern of $H_{max} > 0.5$ m on a very long stretch of the coast in southern Italy and northern Greece, whereas an earthquake of the same size in the Ionian Island Transform Fault Zone (fault group B) produces $H_{max} > 0.5$ m only at few localities (southernmost tip of Apulia and the Ionian Islands). On the other hand, the MFD constrained by tectonic moment rate predicts that the frequency of an $M_w \geq 7$ earthquake in the Ionian Island Transform Fault Zone is about ten times higher than that in the Hellenides Fold-and-thrust Belt.

In the Calabrian Accretionary Wedge (fault group C), the predicted frequency of $M_w \geq 7$ earthquakes is significant as well as the pattern of $H_{max} > 0.5$ m produced on the coasts of southern Italy. However, in this case the tectonically constrained MFD compared with rates of observed earthquakes is an open issue. Are those faults really seismogenic? Given the peculiar mechanical properties of rocks and the modes of tectonic loading in accretionary wedges, is the theoretical MFD a really good descriptor of seismic activity? These very basic knowledge uncertainties are reflected in the classification of these fault sources, as case #5 of our hierarchical justification level scheme for both earthquake and tsunami generation (see Fig. 4, Tables A1 and A2). An approach to the compilation of fault sources that incorporates only sources derived from empirical data on earthquakes and tsunamis implies that fault sources with justification level #5, #6, and possibly, #4 would be totally neglected in the hazard study (see logic-tree branches in Fig. 2. Another open issue is the comparison between the tectonically constrained MFD and observed earthquakes in the Sicily–Tunisia Graben (fault group D). In this case, there exist examples of analog areas, such as the Rhine Graben in northwestern Europe, that address the seismogenic potential in such tectonic setting through paleoseismic studies (Vanneste et al., 2013), filling this gap of knowledge in the open sea would be extremely challenging. This area, however, from our analysis will likely be the one that poses the least hazard for a combination of reasons. On the one hand, the earthquake activity rate that may produce significant tsunami waves is lower than that of all other fault sources. An $M_w = 7$ earthquake, a magnitude at the very uppermost moment bound of the MFD, produces $H_{max} > 0.5$ m only at few sites in the Sicily Channel. The bathymetric effects also cause the waning of waves that propagate across the Malta Escarpment into the eastern side of the basin.

In the case of subduction zones (Hellenic and Calabrian arcs), we examined the epistemic uncertainties in more detail with regards to parameters that control the construction of the MFD, such as the seismogenic bottom depth, long-term aseismic factor, and moment upper bound. The variability of these parameters, on the basis of available data and studies, produces very different earthquake activity rates. Although the pattern of $H_{max} > 0.5$ m produced by $M_w = 7$ earthquakes in the subduction interface of both subduction zones are comparable to those on the corresponding crustal fault sources, the frequency of $M_w \geq 7$ earthquakes in the Hellenic Arc subduction interface is much higher than that of any other fault group in the area. The effects of the epistemic uncertainties of these subduction zones can also be looked at from the perspective of a specific temporal horizon. For instance, with reference to having one earthquake in 100 yr, the ensemble of MFDs for the Hellenic Arc that takes into account all the considered epistemic uncertainties includes earthquakes ranging in size from $M_w > 7$ to $M_w > 8$. Considering the dramatic difference in H_{max} patterns produced in the two pairs of scenarios, we calculated (Fig. 6g, h, i,j) that one can also expect a high uncertainty in the final hazard computation.

In analogy with the use of fault sources in PSHA, other epistemic uncertainties are encountered at each step of the fault characterization. As an example, we calculated prospective activity rates, in the form of MFD restrained with an upper moment bound (Pareto) constrained by applying scaling laws to fault dimensions and balanced with tectonic moment rates. Other recurrence models should also be applied and global vs. regional constraints to MFD should be tested. In addition, all geometric and kinematic parameters, as well as the fault mechanical properties, have their own epistemic uncertainties that were not treated here since they deserve further specific investigations.

In order to perform a comprehensive PTHA study, the contribution to the hazard from all possible fault sources should be incorporated, not just fault sources here classified as Type 1. Lack of data or controversial interpretations of available data may prevent the full characterization of fault sources (e.g. Types 2 and 3; Sect. 2) and different strategies can be adopted to define some default parameters or reconcile alternative interpretations. These strategies, however, will only provide an opportunity to run the hazard calculations, while the epistemic uncertainty of those potential fault sources remains clearly earmarked. With this goal in mind, we reported as an illustrative example the possible treatment of such epistemic uncertainties in a logic tree scheme (Fig. 2). We did not explore the possible choices of a weighting scheme to be associated to this classification. Disaggregation analysis could help highlight the contribution to the hazard from fault sources with higher uncertainty and promote their reappraisal to compensate the lack of knowledge. Disaggregation, however, can only be performed after the hazard analysis is completed. For a better guidance, on how to handle the epistemic uncertainties beforehand, one could use sensitivity analysis explicitly carried out for tsunami metrics.

Appendix A

Table A1. Justification level for crustal and subduction fault sources (see Fig. 3 for location). In case the reason for a level attribution fails, potential upgrade or downgrade options are shown beside each case. Unless otherwise noted, all earthquakes mentioned here are from SHEEC (Stucchi et al., 2012) and EMEC (Grünthal and Wahlström, 2012) catalogs.

Crustal fault sources							
ID	Name	S-level	Notes*	Upgrade/Downgrade	T-level	Notes*	Upgrade/Downgrade
A1	Sazani	5	Fault displaces young sedimentary units and kinematics is compatible with current stress regime.	This could be the source of the 1930 earthquake and be upgraded to class 1.	5	Fault displaces young sedimentary units at shallow depth beneath the seafloor and kinematics is compatible with current stress regime.	Could be upgraded to class 4 if one considers the tsunami observed during the March 1270, $M = 6.7$, Durres earthquake, which occurred on another fault of the same fault system.
A2	Albania offshore	5	Fault displaces young sedimentary units and kinematics is compatible with current stress regime.	Could be upgraded to class 4 if A1 is upgraded to class 1, or if considering other fault sources to the north.	5	Fault displaces young sedimentary units at shallow depth beneath the seafloor and kinematics is compatible with current stress regime.	Could be upgraded to class 4 if one considers the tsunami observed during the March 1270, $M = 6.7$, Durres earthquake, which occurred on another fault of the same fault system.
A3	Seman Coastal	5	Fault displaces young sedimentary units and kinematics is compatible with current stress regime.	Could be upgraded to class 4 if A1 is upgraded to class 1, or if considering other fault sources to the north.	5	Fault displaces young sedimentary units at shallow depth beneath the seafloor and kinematics is compatible with current stress regime.	Could be upgraded to class 4 if one considers the tsunami observed during the March 1270, $M = 6.7$, Durres earthquake, which occurred on another fault of the same fault system.
A4	Vlora	5	Fault displaces young sedimentary units and kinematics is compatible with current stress regime.	Could be upgraded to class 4 if A1 is upgraded to class 1, or if considering other fault sources to the north.	5	Fault displaces young sedimentary units at shallow depth beneath the seafloor and kinematics is compatible with current stress regime.	Could be upgraded to class 4 if one considers the tsunami observed during the March 1270, $M = 6.7$, Durres earthquake, which occurred on another fault of the same fault system.
A5	Kerkyra	3	Two Holocene raised notches interpreted as coseismic uplift events were detected and dated by Pirazzoli et al. (1994) along the coast of Kerkyra Island.	More information is needed about the 29 June 2007, $M = 5.6$, earthquake to upgrade the fault source to class 1.	5	Fault displaces young sedimentary units at shallow depth beneath the seafloor and kinematics is compatible with current stress regime.	More information is needed about known historical tsunamis to upgrade the fault to class 2.
A6	Kerkyra offshore	4	Fault is part of a system with another fault (A5) in class 3.		5	Fault displaces young sedimentary units at shallow depth beneath the seafloor and kinematics is compatible with current stress regime.	Could be upgraded to class 4 if A5 is upgraded to class 2.
B1	Lefkada	1	Source of the 2003, $M = 6.2$, and of the 1948, $M = 6.5$, earthquakes (Papadimitriou et al., 2006).		1	Tsunami waves were observed during the 1948, $M = 6.5$, earthquake (Papadimitriou et al., 2006; NOAA).	Part of the fault is onshore.
B2	Cephalonia	1	Source of the 1983, $M = 7.0$, earthquake (Louvari et al., 1999).	Could also be the source of the 1867 earthquake and be at least of class 2.	1	Tsunami associated with the 17 January 1983, $M = 7.0$, earthquake (NOAA).	Part of the fault is onshore.
B3	Achaia	1	Source of the 2008, $M = 6.4$, earthquake (Ganas et al., 2009).		4	Fault is part of a system with other faults in class 1.	The northeastern part of the fault is onshore.
B4	Mediterranean North	4	Fault is part of a system with other faults (B1–3) in class 1.	Could be upgraded to class 1 if associated with one of the several earthquakes in the area.	4	Fault is part of a system with other faults in class 1.	Shallow active fault entirely offshore.
B5	Zakinthos offshore	4	Fault is part of a system with other faults (B1–3) in class 1.		4	Fault is part of a system with other faults in class 1.	Shallow active fault entirely offshore.

* The term "young" for sedimentary units may refer to different geologic ages for different faults; it is most often the Quaternary, although at times may simply refer to the youngest sedimentary units encountered in the area.

Table A1. Continued.

ID	Name	S-level	Notes*	Upgrade/Downgrade	T-level	Notes*	Upgrade/Downgrade
				Crustal fault sources			
C1	Crotone–Rossano	5	Fault displaces young sedimentary units and kinematics is compatible with current stress regime.	Could be upgraded to class 2 if associated with the 1832 earthquake.	5	Shallow active fault entirely offshore.	
C2	Calabria offshore SE	5	Fault displaces young sedimentary units and kinematics is compatible with deformation of the Calabrian Accretionary Wedge.		5	Shallow active fault entirely offshore.	Could be upgraded to class 4 if the earthquakes of 1693 or 1905 (generating tsunamis) are associated to the subduction plane.
C3	Calabria offshore S		Fault displaces young sedimentary units and kinematics is compatible with deformation of the Calabrian Accretionary Wedge.		5	Shallow active fault entirely offshore.	Could be upgraded to class 4 if the earthquakes of 1693 or 1905 (generating tsunamis) are associated to the subduction plane.
C4	Calabria offshore SW		Fault displaces young sedimentary units and kinematics is compatible with deformation of the Calabrian Accretionary Wedge.		5	Shallow active fault entirely offshore.	Could be upgraded to class 4 if the earthquakes of 1693 or 1905 (generating tsunamis) are associated to the subduction plane.
C5	Calabria offshore NE		Fault displaces young sedimentary units and kinematics is compatible with deformation of the Calabrian Accretionary Wedge.		5	Shallow active fault entirely offshore.	Could be upgraded to class 4 if the earthquakes of 1693 or 1905 (generating tsunamis) are associated to the subduction plane.
C6	Calabria offshore NW	5	Fault displaces young sedimentary units and kinematics is compatible with deformation of the Calabrian Accretionary Wedge.		5	Shallow active fault entirely offshore.	Could be upgraded to class 4 if the earthquakes of 1693 or 1905 (generating tsunamis) are associated to the subduction plane.
D1	PantelleriaN	5	Fault displaces young sedimentary units and kinematics is compatible with current stress regime.		5	Shallow active fault entirely offshore.	
D2	MaltaN	5	Fault displaces young sedimentary units and kinematics is compatible with current stress regime.		5	Shallow active fault entirely offshore.	
D3	LinosaN	5	Fault displaces young sedimentary units and kinematics is compatible with current stress regime.		5	Shallow active fault entirely offshore.	
D4	LampedusaN	5	Fault displaces young sedimentary units and kinematics is compatible with current stress regime.		5	Shallow active fault entirely offshore.	
				Subduction fault sources			
S1	Calabrian Arc	5	GPS velocity field reveals active convergence between the African and European plates.	Could be upgraded to class 2 if the 1693 or 1905 earthquakes are associated with the subduction plane.	5	Shallower part of the subduction interface is offshore.	Could be upgraded to class 2 if the 1693 or 1905 earthquakes (which generated tsunamis) are associated with the subduction plane.
S2	Hellenic Arc	1	Several instrumentally recorded earthquakes.	Historical earthquakes, such as the 365 or 1303, would confirm at least class 2.	2	Tsunami associated with the 21 July 365, $M = 8+$, earthquake.	Could be downgraded to class 4 if the 21 July 365, $M = 8+$, earthquake is associated with other faults of the subduction system.

* The term "young" for sedimentary units may refer to different geologic ages for different faults; it is most often the Quaternary, although at times may simply refer to the youngest sedimentary units encountered in the area.

Appendix B

Table B1. Summary of various solutions for the source of the 11 January 1693 tsunami.

Fault model[c]	Lat[a]	Long[a]	Distance to Augusta[b]	Bearing to Augusta[b]	*L*	*W*	Strike	Dip	Rake	Slip	Depth to top	Depth to bottom	Notes
1	37.055	15.330	22	334	50	15	346	90	dip slip	6.2	2	17	Located onshore (west side up).
2	37.264	14.979	22	100	40	10	250	60	300	3.4	2.7	11.4	Solution "SL1" fault; partially onshore.
3	37.358	15.026	22	130	30	15	67.5	30	270	8	3.0	10.5	Solution "SL2"; fault partially onshore.
4	36.476	17.021	181	298	120	170	225	5	90	2	5	20	Modelled with non uniform slip.
5	37.277	15.396	16	252	28.5	16.5	330–360	28	270	5	0.5	8.2	Composed by subfaults of 5.8–10.2 km long.

[a] Fault coordinates (columns Lat, Long) are those of the top-middle point.
[b] Distance and bearing to the town of Augusta are from the fault top-middle point to a point with coordinates 15.22° E, 37.23° N.
[c] 1 – Piatanesi and Tinti (1998); 2, 3 – Tinti et al. (2001); 4 – Gutscher et al. (2006); 5 – Argnani et al. (2012).

Acknowledgements. We thank three anonymous reviewers for their constructive comments that improved the quality of the paper. We also thank Pierfrancesco Burrato, Alina Polonia, Patrizio Petricca, and Paola Vannoli for providing insights on several fault sources of southern Italy. This work was supported by the EC-Research Framework programme FP7, Seismic Hazard Harmonization in Europe, Grant Agreement No. 226769 and the Flagship Project RITMARE – The Italian Research for the Sea – coordinated by the Italian National Research Council and funded by the Italian Ministry of Education, University and Research within the National Research Program 2011–2013.

Edited by: G. Boni
Reviewed by: three anonymous referees

References

Ambraseys, N. and Synolakis, C.: Tsunami Catalogs for the Eastern Mediterranean, Revisited, J. Earthq. Eng., 14, 309–330, doi:10.1080/13632460903277593, 2010.

Annaka, T., Satake, K., Sakakiyama, T., Yanagisawa, K., and Shuto, N.: Logic-tree Approach for Probabilistic Tsunami Hazard Analysis and its Applications to the Japanese Coasts, Pure Appl. Geophys., 164, 577–592, doi:10.1007/s00024-006-0174-3, 2007.

Argnani, A., Armigliato, A., Pagnoni, G., Zaniboni, F., Tinti, S., and Bonazzi, C.: Active tectonics along the submarine slope of south-eastern Sicily and the source of the 11 January 1693 earthquake and tsunami, Nat. Hazards Earth Syst. Sci., 12, 1311–1319, doi:10.5194/nhess-12-1311-2012, 2012.

Basili, R., Valensise, G., Vannoli, P., Burrato, P., Fracassi, U., Mariano, S., Tiberti, M. M., and Boschi, E.: The Database of Individual Seismogenic Sources (DISS), version 3: Summarizing 20 years of research on Italy's earthquake geology, Tectonophysics, 453, 20–43, doi:10.1016/j.tecto.2007.04.014, 2008.

Becker, D. and Meier, T.: Seismic Slip Deficit in the Southwestern Forearc of the Hellenic Subduction Zone, B. Seismol. Soc. Am., 100, 325–342, doi:10.1785/0120090156, 2010.

Benetatos, C., Kiratzi, A., Papazachos, C., and Karakaisis, G.: Focal mechanisms of shallow and intermediate depth earthquakes along the Hellenic Arc, J. Geodyn., 37, 253–296, doi:10.1016/j.jog.2004.02.002, 2004.

Benetatos, C., Dreger, D., and Kiratzi, A.: Complex and Segmented Rupture Associated with the 14 August 2003 Mw 6.2 Lefkada, Ionian Islands, Earthquake, B. Seismol. Soc. Am., 97, 35–51, doi:10.1785/0120060123, 2007.

Bilek, S. L. and Lay, T.: Rigidity variations with depth along interplate megathrust faults in subduction zones, Nature, 400, 443, doi:10.1038/22739, 1999.

Billi, A., Funiciello, R., Minelli, L., Faccenna, C., Neri, G., Orecchio, B., and Presti, D.: On the cause of the 1908 Messina tsunami, southern Italy, Geophys. Res. Lett., 35, L06301, doi:10.1029/2008GL033251, 2008.

Bohnhoff, M., Makris, J., Papanikolaou, D., and Stavrakakis, G.: Crustal investigation of the Hellenic subduction zone using wide aperture seismic data, Tectonophysics, 343, 239–262, doi:10.1016/S0040-1951(01)00264-5, 2001.

Bohnhoff, M., Harjes, H.-P., and Meier, T.: Deformation and stress regimes in the Hellenic subduction zone from focal Mechanisms, J. Seismol., 9, 341—366, doi:10.1007/s10950-005-8720-5, 2005.

Budnitz, R. J., Apostolakis, G., Boore, D. M., Cluff, L. S., Coppersmith, K. J., Cornell, C. A., and Morris, P. A.: Recommendations for probabilistic seismic hazard analysis: guidance on uncertainty and the use of experts, US Nuclear Regulatory Commission, Washington, D.C., NUREG/CR-6372, Volume 2, 1997.

Burbidge, D., Cummins, P., Mleczko, R., and Thio, H.: A Probabilistic Tsunami Hazard Assessment for Western Australia, Pure Appl. Geophys., 165, 2059–2088, doi:10.1007/s00024-008-0421-x, 2008.

Capitanio, F. A., Faccenna, C., and Funiciello, R.: The opening of Sirte basin: Result of slab avalanching?, Earth Planet. Sc. Lett., 285, 210–216, doi:10.1016/j.epsl.2009.06.019, 2009.

Capozzi, R., Artoni, A., Torelli, L., Lorenzini, S., Oppo, D., Mussoni, P., and Polonia, A.: Neogene to Quaternary tectonics and mud diapirism in the Gulf of Squillace (Crotone-Spartivento Basin, Calabrian Arc, Italy), Mar. Petrol. Geol., 35, 219–234, doi:10.1016/j.marpetgeo.2012.01.007, 2012.

Casten, U. and Snopek, K.: Gravity modelling of the Hellenic subduction zone – a regional study, Tectonophysics, 417, 183–200, doi:10.1016/j.tecto.2005.11.002, 2006.

Chamot-Rooke, N., Rabaute, A., and Kreemer, C.: Western Mediterranean Ridge mud belt correlates with active shear strain at the prism-backstop geological contact, Geology, 33, 861–864, doi:10.1130/g21469.1, 2005.

Chiarabba, C., Jovane, L., and DiStefano, R.: A new view of Italian seismicity using 20 years of instrumental recordings, Tectonophysics, 395, 251–268, doi:10.1016/j.tecto.2004.09.013, 2005.

Chiarabba, C., De Gori, P., and Speranza, F.: The southern Tyrrhenian subduction zone: Deep geometry, magmatism and Plio-Pleistocene evolution, Earth Planet. Sc. Lett., 268, 408–423, doi:10.1016/j.epsl.2008.01.036, 2008.

Civile, D., Lodolo, E., Accettella, D., Geletti, R., Ben-Avraham, Z., Deponte, M., Facchin, L., Ramella, R., and Romeo, R.: The Pantelleria graben (Sicily Channel, Central Mediterranean): An example of intraplate "passive" rift, Tectonophysics, 490, 173–183, doi:10.1016/j.tecto.2010.05.008, 2010.

Corti, G., Cuffaro, M., Doglioni, C., Innocenti, F., and Manetti, P.: Coexisting geodynamic processes in the Sicily Channel, GSA Special Papers, 409, 83–96, doi:10.1130/2006.2409(05), 2006.

D'Agostino, N. and Selvaggi, G.: Crustal motion along the Eurasia-Nubia plate boundary in the Calabrian Arc and Sicily and active extension in the Messina Straits from GPS measurements, J. Geophys. Res., 109, B11402, doi:10.1029/2004JB002998, 2004.

D'Agostino, N., D'Anastasio, E., Gervasi, A., Guerra, I., Nedimovi, R., M., Seeber, L., and Steckler, M.: Forearc extension and slow rollback of the Calabrian Arc from GPS measurements, Geophys. Res. Lett., 38, L17304, doi:10.1029/2011GL048270, 2011.

Del Ben, A., Barnaba, C., and Taboga, A.: Strike-slip systems as the main tectonic features in the Plio-Quaternary kinematics of the Calabrian Arc, Mar. Geophys. Res., 29, 1–12, doi:10.1007/s11001-007-9041-6, 2008.

Devoti, R., Riguzzi, F., Cuffaro, M., and Doglioni, C.: New GPS constraints on the kinematics of the Apennines subduction, Earth Planet. Sc. Lett., 273, 163–174, doi:10.1016/j.epsl.2008.06.031, 2008.

Dilek, Y. and Sandvol, E.: Seismic structure, crustal architecture and tectonic evolution of the Anatolian-African Plate Boundary and the Cenozoic Orogenic Belts in the Eastern Mediterranean Region, Geological Society, London, Special Publications, 327, 127–160, doi:10.1144/sp327.8, 2009.

DISS Working Group: Database of Individual Seismogenic Sources (DISS), version 3.1.1: a compilation of potential sources for earthquakes larger than M 5.5 in Italy and surrounding areas, available at: http://diss.rm.ingv.it/diss/ (last access: 28 February 2013), 2010.

Drakos, A. G. and Stiros, S. C.: The AD 365 earthquake. From legend to modelling, Bulletin of the Geological Society of Greece, 34, 1417–1424, 2001.

Dziewonski, A. M. and Anderson, D. L. : Preliminary reference Earth model, Phys. Earth Planet. In., 25, 297–356, 1981.

Feng, L., Newman, A. V., Farmer, G. T., Psimoulis, P., and Stiros, S. C.: Energetic rupture, coseismic and post-seismic response of the 2008 M_w 6.4 Achaia-Elia Earthquake in northwestern Peloponnese, Greece: an indicator of an immature transform fault zone, Geophys. J. Int., 183, 103–110, doi:10.1111/j.1365-246X.2010.04747.x, 2010.

Finetti, I. R.: The Calabrian Arc and subducting Ionian slab from new crop seismic data, in: CROP Project, Deep Seismic Exploration of the Central Mediterranean Region and Italy, edited by: Finetti, I. R., Elsevier, 393–412, 2005.

Finetti, I. R. and Del Ben, A.: Crustal tectono-stratigraphic setting of the Adriatic Sea from new CROP seismic data, in: CROP Project, Deep Seismic Exploration of the Central Mediterranean and Italy, edited by: Finetti, I. R., Elsevier, 519–547, 2005a.

Finetti, I. R. and Del Ben, A.: Crustal tectono-stratigraphic setting of the Pelagian foreland from new CROP seismic data, in: CROP Project, Deep Seismic Exploration of the Central Mediterranean and Italy, edited by: Finetti, I. R., Elsevier, 581–595, 2005b.

Ganas, A. and Parsons, T.: Three-dimensional model of Hellenic Arc deformation and origin of the Cretan uplift, J. Geophys. Res., 114, B06404, doi:10.1029/2008JB005599, 2009.

Ganas, A., Serpelloni, E., Drakatos, G., Kolligri, M., Adamis, I., Tsimi, C., and Batsi, E.: The Mw 6.4 SW-Achaia (Western Greece) Earthquake of 8 June 2008: Seismological, Field, GPS Observations, and Stress Modeling, J. Earthq. Eng., 13, 1101–1124, doi:10.1080/13632460902933899, 2009.

Geist, E. L.: Phenomenology of Tsunamis, in: Statistical Properties from Generation to Runup, Chapter 3, edited by: Dmowska, R., Adv. Geophys., 51, 107–169, doi:10.1016/S0065-2687(09)05108-5, 2009.

Geist, E. L. and Parsons, T.: Probabilistic Analysis of Tsunami Hazards, Nat. Hazards, 37, 277–314, doi:10.1007/s11069-005-4646-z, 2006.

Gerardi, F., Barbano, M. S., De Martini, P. M., and Pantosti, D.: Discrimination of Tsunami Sources (Earthquake versus Landslide) on the Basis of Historical Data in Eastern Sicily and Southern Calabria, B. Seismol. Soc. Am., 98, 2795–2805, doi:10.1785/0120070192, 2008.

Gesret, A., Laigle, M., Diaz, J., Sachpazi, M., and Hirn, A.: The oceanic nature of the African slab subducted under Peloponnesus: thin-layer resolution from multiscale analysis of teleseismic P-to-S converted waves, Geophys. J. Int., 183, 833–849, doi:10.1111/j.1365-246X.2010.04738.x, 2010.

Gesret, A., Laigle, M., Diaz, J., Sachpazi, M., Charalampakis, M., and Hirn, A.: Slab top dips resolved by teleseismic converted waves in the Hellenic subduction zone, Geophys. Res. Lett., 38, 20, doi:10.1029/2011GL048996, 2011.

Giacomuzzi, G., Chiarabba, C., and De Gori, P.: Linking the Alps and Apennines subduction systems: New constraints revealed by high-resolution teleseismic tomography, Earth Planet. Sc. Lett., 301, 531–543, doi:10.1016/j.epsl.2010.11.033, 2011.

González, F. I., Geist, E. L., Jaffe, B., Kânoğlu, U., Mofjeld, H., Synolakis, C. E., Titov, V. V., Arcas, D., Bellomo, D., Carlton, D., Horning, T., Johnson, J., Newman, J., Parsons, T., Peters, R., Peterson, C., Priest, G., Venturato, A., Weber, J., Wong, F., and Yalciner, A.: Probabilistic tsunami hazard assessment at Seaside, Oregon, for near- and far-field seismic sources, J. Geophys. Res., 114, C11023, doi:10.1029/2008JC005132, 2009.

Grezio, A., Marzocchi, W., Sandri, L., and Gasparini, P.: A Bayesian procedure for Probabilistic Tsunami Hazard Assessment, Nat. Hazards, 53, 159–174, doi:10.1007/s11069-009-9418-8, 2010.

Grezio, A., Sandri, L., Marzocchi, W., Argnani, A., Gasparini, P., and Selva, J.: Probabilistic tsunami hazard assessment for Messina Strait Area (Sicily, Italy), Nat. Hazards, 64, 329–358, doi:10.1007/s11069-012-0246-x, 2012.

Grünthal, G. and Wahlström, R.: The European-Mediterranean Earthquake Catalogue (EMEC) for the last millennium, J. Seismol., 16, 535–570, doi:10.1007/s10950-012-9302-y, 2012.

Guidoboni, E., Comastri, A., and Traina, G.: Catalogue of Ancient Earthquakes in the Mediterranean Area up to the 10th Century, SGA, 1994.

Guidoboni, E., Ferrari, G., Mariotti, D., Comastri, A., Tarabusi, G., and Valensise, G.: CFTI4Med, Catalogue of Strong Earthquakes in Italy (461 B.C.–1997) and Mediterranean Area (760 B.C.–1500), INGV-SGA, 2007.

Gutscher, M. A., Roger, J., Baptista, M. A., Miranda, J. M., and Tinti, S.: Source of the 1693 Catania earthquake and tsunami (southern Italy): New evidence from tsunami modeling of a locked subduction fault plane, Geophys. Res. Lett., 33, L08309, doi:10.1029/2005GL025442, 2006.

Haller, K. M. and Basili, R.: Developing Seismogenic Source Models Based on Geologic Fault Data, Seismol. Res. Lett., 82, 519–525, doi:10.1785/gssrl.82.4.519, 2011.

Hatzfeld, D. and Martin, C.: Intermediate depth seismicity in the Aegean defined by teleseismic data, Earth Planet. Sc. Lett., 113, 267–275, doi:10.1016/0012-821X(92)90224-J, 1992.

Heuret, A., Lallemand, S., Funiciello, F., Piromallo, C., and Faccenna, C.: Physical characteristics of subduction interface type seismogenic zones revisited, Geochem. Geophy. Geosy., 12, Q01004, doi:10.1029/2010GC003230, 2011.

Hollenstein, C., Müller, M. D., Geiger, A., and Kahle, H. G.: Crustal motion and deformation in Greece from a decade of GPS measurements, 1993–2003, Tectonophysics, 449, 17–40, doi:10.1016/j.tecto.2007.12.006, 2008.

Howe, T. C. and Bird, P.: Exploratory models of long-term crustal flow and resulting seismicity in the Alpine-Aegean orogen, Tectonics, 29, TC4023, doi:10.1029/2009TC002565, 2010.

Huguen, C., Mascle, J., Chaumillon, E., Woodside, J. M., Benkhelil, J., Kopf, A., and Volkonskaïa, A.: Deformational styles of the eastern Mediterranean Ridge and surroundings from combined swath mapping and seismic reflection profiling, Tectonophysics, 343, 21–47, doi:10.1016/S0040-1951(01)00185-8, 2001.

Jackson, J. and McKenzie, D.: The relationship between plate motions and seismic moment tensors, and the rates of active deformation in the Mediterranean and Middle East, Geophys. J., 93, 45–73, doi:10.1111/j.1365-246X.1988.tb01387.x, 1988.

Jongsma, D., van Hinte, J. E., and Woodside, J. M.: Geologic structure and neotectonics of the North African Continental Margin south of Sicily, Mar. Petrol. Geol., 2, 156–179, 1985.

Kagan, Y. Y.: Seismic moment distribution revisited: I. Statistical results, Geophys. J. Int., 148, 520–541, doi:10.1046/j.1365-246x.2002.01594.x, 2002a.

Kagan, Y. Y.: Seismic moment distribution revisited: II. Moment conservation principle, Geophys. J. Int., 149, 731–754, doi:10.1046/j.1365-246X.2002.01671.x, 2002b.

Kahle, H., Gert, Müller, M. V., and Veis, G.: Trajectories of crustal deformation of western Greece from GPS observations 1989–1994, Geophys. Res. Lett., 23, 677–680, doi:10.1029/96GL00264, 1996.

Kanamori, H. and Brodsky, E. E.: The physics of earthquakes, Rep. Prog. Phys., 67, 1429, doi:10.1088/0034-4885/67/8/R03, 2004.

Kastens, K. A.: Rate of outward growth of the Mediterranean ridge accretionary complex, Tectonophysics, 199, 25–50, 1991.

Kimura, G., Moore, G. F., Strasser, M., Screaton, E., Curewitz, D., Streiff, C., and Tobin, H.: Spatial and temporal evolution of the megasplay fault in the Nankai Trough, Geochem. Geophy. Geosy., 12, Q0A008, doi:10.1029/2010GC003335, 2011.

Kokinou, E., Kamberis, E., Vafidis, A., Monopolis, D., Ananiadis, G., and Zelilidis, A.: Deep seismic reflection data from offshore western Greece: a new crustal model for the Ionian Sea, J. Petrol. Geol., 28, 185–202, 2005.

Kokinou, E., Papadimitriou, E., Karakostas, V., Kamberis, E., and Vallianatos, F.: The Kefalonia Transform Zone (offshore Western Greece) with special emphasis to its prolongation towards the Ionian Abyssal Plain, Mar. Geophys. Res., 27, 241–252, doi:10.1007/s11001-006-9005-2, 2006.

Kreemer, C. and Chamot-Rooke, N.: Contemporary kinematics of the southern Aegean and the Mediterranean Ridge, Geophys. J. Int., 157, 1377–1392, doi:10.1111/j.1365-246X.2004.02270.x, 2004.

Kukowski, N., Lallemand, S. E., Malavieille, J., Gutscher, M.-A., and Reston, T. J.: Mechanical decoupling and basal duplex formation observed in sandbox experiments with application to the Western Mediterranean Ridge accretionary complex, Mar. Geol., 186, 29–42, doi:10.1016/S0025-3227(02)00171-8, 2002.

Laigle, M., Hirn, A., Sachpazi, M., and Clément, C.: Seismic coupling and structure of the Hellenic subduction zone in the Ionian Islands region, Earth Planet. Sc. Lett., 200, 243–253, doi:10.1016/S0012-821X(02)00654-4, 2002.

Laigle, M., Sachpazi, M., and Hirn, A.: Variation of seismic coupling with slab detachment and upper plate structure along the western Hellenic subduction zone, Tectonophysics, 391, 85–95, doi:10.1016/j.tecto.2004.07.009, 2004.

Leonard, M.: Earthquake Fault Scaling: Self-Consistent Relating of Rupture Length, Width, Average Displacement, and Moment Release, B. Seismol. Soc. Am., 100, 1971–1988, doi:10.1785/0120090189, 2010.

Li, X., Bock, G., Vafidis, A., Kind, R., Harjes, H. P., Hanka, W., Wylegalla, K., Van Der Meijde, M., and Yuan, X.: Receiver function study of the Hellenic subduction zone: imaging crustal thickness variations and the oceanic Moho of the descending African lithosphere, Geophys. J. Int., 155, 733–748, doi:10.1046/j.1365-246X.2003.02100.x, 2003.

Lorito, S., Tiberti, M. M., Basili, R., Piatanesi, A., and Valensise, G.: Earthquake-generated tsunamis in the Mediterranean Sea: Scenarios of potential threats to Southern Italy, J. Geophys. Res., 113, B01301, doi:10.1029/2007JB004943, 2008.

Louvari, E., Kiratzi, A. A., and Papazachos, B. C.: The Cephalonia Transform Fault and its extension to western Lefkada Island (Greece), Tectonophysics, 308, 223–236, doi:10.1016/S0040-1951(99)00078-5, 1999.

Louvari, E., Kiratzi, A., Papazachos, B., and Hatzidimitriou, P.: Fault-plane Solutions Determined by Waveform Modeling Confirm Tectonic Collision in the Eastern Adriatic, Pure Appl. Geo-

phys., 158, 1613–1637, 2001.

Løvholt, F., Bungum, H., Harbitz, C. B., Glimsdal, S., Lindholm, C. D., and Pedersen, G.: Earthquake related tsunami hazard along the western coast of Thailand, Nat. Hazards Earth Syst. Sci., 6, 979–997, doi:10.5194/nhess-6-979-2006, 2006.

Løvholt, F., Pedersen, G., Bazin, S., Kühn, D., Bredesen, R. E., and Harbitz, C.: Stochastic analysis of tsunami runup due to heterogeneous coseismic slip and dispersion, J. Geophys. Res., 117, C03047, doi:10.1029/2011JC007616, 2012a.

Løvholt, F., Kühn, D., Bungum, H., Harbitz, C. B., and Glimsdal, S.: Historical tsunamis and present tsunami hazard in eastern Indonesia and the southern Philippines, J. Geophys. Res., 117, B09310, doi:10.1029/2012JB009425, 2012b.

Makris, J. and Yegorova, T.: A 3-D density-velocity model between the Cretan Sea and Libya, Tectonophysics, 417, 201–220, doi:10.1016/j.tecto.2005.11.003, 2006.

McKenzie, D.: Active tectonics of the Alpine-Himalayan belt: the Aegean Sea and surrounding regions, Geophys. J. Roy. Astr. S., 55, 217–254, doi:10.1111/j.1365-246X.1978.tb04759.x, 1978.

Meier, T., Rische, M., Endrun, B., Vafidis, A., and Harjes, H. P.: Seismicity of the Hellenic subduction zone in the area of western and central Crete observed by temporary local seismic networks, Tectonophysics, 383, 149–169, doi:10.1016/j.tecto.2004.02.004, 2004.

Meier, T., Becker, D., Endrun, B., Rische, M., Bohnhoff, M., Stöckhert, B., and Harjes, H. P.: A model for the Hellenic subduction zone in the area of Crete based on seismological investigations, Geol. Soc. Spec. Publ., 291, 183–199, doi:10.1144/sp291.9, 2007.

Merlini, S., Cantarella, G., and Doglioni, C.: On the seismic profile Crop M5 in the Ionian Sea, B. Soc. Geol. Ital., 119, 227–236, 2000.

Minelli, L. and Faccenna, C.: Evolution of the Calabrian accretionary wedge (central Mediterranean), Tectonics, 29, TC4004, doi:10.1029/2009tc002562, 2010.

Mitsoudis, D. A., Flouri, E. T., Chrysoulakis, N., Kamarianakis, Y., Okal, E. A., and Synolakis, C. E.: Tsunami hazard in the southeast Aegean Sea, Coast. Eng., 60, 136–148, doi:10.1016/j.coastaleng.2011.09.004, 2012.

National Geophysical Data Center/World Data System (NGDC/WDS) Global Historical Tsunami Database, Boulder, CO, USA, available at http://www.ngdc.noaa.gov/hazard/tsu_db.shtml, last access: 28 February 2013.

Neri, A., Aspinall, W. P., Cioni, R., Bertagnini, A., Baxter, P. J., Zuccaro, G., Andronico, D., Barsotti, S., Cole, P. D., Esposti Ongaro, T., Hincks, T. K., Macedonio, G., Papale, P., Rosi, M., Santacroce, R., and Woo, G.: Developing an Event Tree for probabilistic hazard and risk assessment at Vesuvius, J. Volcanol. Geoth. Res.h, 178, 397–415, doi:10.1016/j.jvolgeores.2008.05.014, 2008.

Okada, Y.: Surface deformation due to shear and tensile faults in a half-space, B. Seismol. Soc. Am., 75, 1135–1154, 1985.

Okada, Y.: Internal deformation due to shear and tensile faults in a half-space, B. Seismol. Soc. Am., 82, 1018–1040, 1992.

Okal, E. A., Borrero, J. C., and Synolakis, C. E.: Evaluation of tsunami risk from regional earthquakes at Pisco, Peru, B. Seismol. Soc. Am., 96, 1634–1648, doi:10.1785/0120050158, 2006.

Okal, E. A. and Synolakis, C. E.: Far-field tsunami hazard from mega-thrust earthquakes in the Indian Ocean, Geophys. J. Int., 172, 995–1015, doi:10.1111/j.1365-246X.2007.03674.x, 2008.

Okal, E. A., Synolakis, C. E., and Kalligeris, N.: Tsunami simulations for regional sources in the South China and adjoining seas, Pure Appl. Geophys., 168, 1153–1173, doi:10.1007/s00024-010-0230-x, 2011.

Papadimitriou, P., Kaviris, G., and Makropoulos, K.: The $M_{\mathrm{w}} = 6.3$ 2003 Lefkada earthquake (Greece) and induced stress transfer changes, Tectonophysics, 423, 73–82, doi:10.1016/j.tecto.2006.03.003, 2006.

Papadopoulos, G. A., Kondopoulou, D. P., Leventakis, G. A., and Pavlides, S. B.: Seismotectonics of the Aegean region, Tectonophysics, 124, 67–84, doi:10.1016/0040-1951(86)90138-1, 1986.

Papazachos, B. C., Papadimitriou, E. E., Kiratzi, A. A., Papazachos, C. B., and Louvari, E. K.: Fault plane solutions in the Aegean Sea and the surrounding area and their tectonic implication, B. Geofis. Teor. Appl., 52, 199–218, 1998.

Papazachos, B. C., Papaioannou, C. A., Papazachos, C. B., and Savvaidis, A. S.: Rupture zones in the Aegean region, Tectonophysics, 308, 205–221, doi:10.1016/S0040-1951(99)00073-6, 1999.

Papazachos, B. C., Karakostas, V. G., Papazachos, C. B., and Scordilis, E. M.: The geometry of the Wadati-Benioff zone and lithospheric kinematics in the Hellenic arc, Tectonophysics, 319, 275–300, doi:10.1016/S0040-1951(99)00299-1, 2000.

Papazachos, C. and Nolet, G.: P and S deep velocity structure of the Hellenic area obtained by robust nonlinear inversion of travel times, J. Geophys. Res., 102, 8349–8367, doi:10.1029/96JB03730, 1997.

Pearce, F. D., Rondenay, S., Sachpazi, M., Charalampakis, M., and Royden, L. H.: Seismic investigation of the transition from continental to oceanic subduction along the western Hellenic Subduction Zone, J. Geophys. Res., 117, B07306, doi:10.1029/2011JB009023, 2012.

Petersen, M. D., Frankel, A. D., Harmsen, S. C., Mueller, C. S., Haller, K. M., Wheeler, R. L., Wesson, R. L., Zeng, Y., Boyd, O. S., Perkins, D. M., Luco, N., Field, E. H., Wills, C. J., and Rukstales, K. S.: Documentation for the 2008 Update of the National Seismic Hazard Maps, USGS Open-File Report 2008-1128, 128 pp., 2008.

Piatanesi, A. and Tinti, S.: A revision of the 1693 eastern Sicily earthquake and tsunami, J. Geophys. Res., 103, 2749–2758, doi:10.1029/97JB03403, 1998.

Pino, N. A., Piatanesi, A., Valensise, G., and Boschi, E.: The 28 December 1908 Messina Straits Earthquake (M_w 7.1): A Great Earthquake throughout a Century of Seismology, Seismol. Res. Lett., 80, 243–259, doi:10.1785/gssrl.80.2.243, 2009.

Pirazzoli, P. A., Thommeret, J., Thommeret, Y., Laborel, J., and Montag-Gioni, L. F.: Crustal block movements from holocene shorelines: Crete and antikythira (Greece), Tectonophysics, 86, 27–43, doi:10.1016/0040-1951(82)90060-9, 1982.

Pirazzoli, P. A., Stiros, S. C., Laborel, J., Laborel-Deguen, F., Arnold, M., Papageorgiou, S., and Morhangel, C.: Late-Holocene shoreline changes related to palaeoseismic events in the Ionian Islands, Greece, The Holocene, 4, 397–405, doi:10.1177/095968369400400407, 1994.

Piromallo, C. and Morelli, A.: P wave tomography of the mantle under the Alpine-Mediterranean area, J. Geophys. Res., 108, 2065, doi:10.1029/2002JB001757, 2003.

Polonia, A., Camerlenghi, A., Davey, F., and Storti, F.: Accretion, structural style and syn-contractional sedimentation in the Eastern Mediterranean Sea, Mar. Geol., 186, 127–144, doi:10.1016/S0025-3227(02)00176-7, 2002.

Polonia, A., Torelli, L., Gasperini, L., and Mussoni, P.: Active faults and historical earthquakes in the Messina Straits area (Ionian Sea), Nat. Hazards Earth Syst. Sci., 12, 2311–2328, doi:10.5194/nhess-12-2311-2012, 2012.

Polonia, A., Torelli, L., Mussoni, P., Gasperini, L., Artoni, A., and Klaeschen, D.: The Calabrian Arc subduction complex in the Ionian Sea: Regional architecture, active deformation, and seismic hazard, Tectonics, 30, TC5018, doi:10.1029/2010TC002821, 2011.

Pondrelli, S., Salimbeni, S., Ekström, G., Morelli, A., Gasperini, P., and Vannucci, G.: The Italian CMT dataset from 1977 to the present, Phys. Earth Planet. In., 159, 286–303, doi:10.1016/j.pepi.2006.07.008, 2006.

Pondrelli, S., Salimbeni, S., Morelli, A., Ekström, G., and Boschi, E.: European-Mediterranean Regional Centroid Moment Tensor catalog: Solutions for years 2003 and 2004, Phys. Earth Planet. In., 164, 90–112, doi:10.1016/j.pepi.2007.05.004, 2007.

Pondrelli, S., Salimbeni, S., Morelli, A., Ekström, G., Postpischl, L., Vannucci, G., and Boschi, E.: European-Mediterranean Regional Centroid Moment Tensor catalog: Solutions for 2005-2008, Phys. Earth Planet. In., 185, 74–81, doi:10.1016/j.pepi.2011.01.007, 2011.

Power, W., Downes, G., and Stirling, M.: Estimation of Tsunami Hazard in New Zealand due to South American Earthquakes, Pure Appl. Geophys., 164, 547–564, doi:10.1007/s00024-006-0166-3, 2007.

Power, W., Wallace, L., Wang, X., and Reyners, M.: Tsunami Hazard Posed to New Zealand by the Kermadec and Southern New Hebrides Subduction Margins: An Assessment Based on Plate Boundary Kinematics, Interseismic Coupling, and Historical Seismicity, Pure Appl. Geophys., 169, 36 pp., doi:10.1007/s00024-011-0299-x, 2012.

Reilinger, R., McClusky, S., Vernant, P., Lawrence, S., Ergintav, S., Cakmak, R., Ozener, H., Kadirov, F., Guliev, I., Stepanyan, R., Nadariya, M., Hahubia, G., Mahmoud, S., Sakr, K., ArRajehi, A., Paradissis, D., Al-Aydrus, A., Prilepin, M., Guseva, T., Evren, E., Dmitrotsa, A., Filikov, S. V., Gomez, F., Al-Ghazzi, R., and Karam, G.: GPS constraints on continental deformation in the Africa-Arabia-Eurasia continental collision zone and implications for the dynamics of plate interactions, J. Geophys. Res., 111, B05411, doi:10.1029/2005JB004051, 2006.

Reilinger, R., McClusky, S., Paradissis, D., Ergintav, S., and Vernant, P.: Geodetic constraints on the tectonic evolution of the Aegean region and strain accumulation along the Hellenic subduction zone, Tectonophysics, 488, 22–30, doi:10.1016/j.tecto.2009.05.027, 2010.

Rontogianni, S.: Comparison of geodetic and seismic strain rates in Greece by using a uniform processing approach to campaign GPS measurements over the interval 1994–2000, J. Geodyn., 50, 381–399, doi:10.1016/j.jog.2010.04.008, 2010.

Rontogianni, S., Konstantinou, K. I., Melis, N. S., and Evangelidis, C. P.: Slab stress field in the Hellenic subduction zone as inferred from intermediate-depth earthquakes, Earth Planets Space, 63, 139–144, doi:10.5047/eps.2010.11.011, 2011.

Royden, L. H. and Papanikolaou, D. J.: Slab segmentation and late Cenozoic disruption of the Hellenic arc, Geochem. Geophy. Geosy., 12, Q03010, doi:10.1029/2010GC003280, 2011.

Selva, J., Costa, A., Marzocchi, W., and Sandri, L.: BET_VH: exploring the influence of natural uncertainties on long-term hazard from tephra fallout at Campi Flegrei (Italy), B. Volcanol., 72, 717–733, doi:10.1007/s00445-010-0358-7, 2010.

Selva, J., Marzocchi, W., Papale, P., and Sandri, L.: Operational eruption forecasting at high-risk volcanoes: the case of Campi Flegrei, Naples, J. Appl. Volcanol., 1, 5, doi:10.1186/2191-5040-1-5, 2012.

Serpelloni, E., Vannucci, G., Pondrelli, S., Argnani, A., Casula, G., Anzidei, M., Baldi, P., and Gasperini, P.: Kinematics of the Western Africa-Eurasia plate boundary from focal mechanisms and GPS data, Geophys. J. Int., 169, 1180–1200, doi:10.1111/j.1365-246X.2007.03367.x, 2007.

Serpelloni, E., Burgmann, R., Anzidei, M., Baldi, P., Mastrolembo Ventura, B., and Boschi, E.: Strain accumulation across the Messina Straits and kinematics of Sicily and Calabria from GPS data and dislocation modeling, Earth Planet. Sc. Lett., 298, 347–360, doi:10.1016/j.epsl.2010.08.005, 2010.

Shaw, B., Ambraseys, N. N., England, P. C., Floyd, M. A., Gorman, G. J., Higham, T. F. G., Jackson, J. A., Nocquet, J. M., Pain, C. C., and Piggott, M. D.: Eastern Mediterranean tectonics and tsunami hazard inferred from the AD 365 earthquake, Nat. Geosci, 1, 268–276, doi:10.1038/ngeo151, 2008.

Shaw, B. and Jackson, J.: Earthquake mechanisms and active tectonics of the Hellenic subduction zone, Geophys. J. Int., 181, 966–984, doi:10.1111/j.1365-246X.2010.04551.x, 2010.

Sodoudi, F., Kind, R., Hatzfeld, D., Priestley, K., Hanka, W., Wylegalla, K., Stavrakakis, G., Vafidis, A., Harjes, H. P., and Bohnhoff, M.: Lithospheric structure of the Aegean obtained from P and S receiver functions, J. Geophys. Res., 111, B12307, doi:10.1029/2005JB003932, 2006.

Sørensen, M. B., Spada, M., Babeyko, A., Wiemer, S., and Grünthal, G.: Probabilistic tsunami hazard in the Mediterranean Sea, J. Geophys. Res., 117, B01305, doi:10.1029/2010JB008169, 2012.

Stirling, M., McVerry, G., Gerstenberger, M., Litchfield, N., Van Dissen, R., Berryman, K., Barnes, P., Wallace, L., Villamor, P., Langridge, R., Lamarche, G., Nodder, S., Reyners, M., Bradley, B., Rhoades, D., Smith, W., Nicol, A., Pettinga, J., Clark, K., and Jacobs, K.: National Seismic Hazard Model for New Zealand: 2010 Update, B. Seismol. Soc. Am., 102, 1514–1542, doi:10.1785/0120110170, 2012.

Stiros, S. C., Pirazzoli, P. A., Laborel, J., and Laborel-Deguen, F.: The 1953 earthquake in Cephalonia (Western Hellenic Arc): coastal uplift and halotectonic faulting, Geophys. J. Int., 117, 834–849, doi:10.1111/j.1365-246X.1994.tb02474.x, 1994.

Strasser, F. O., Arango, M. C., and Bommer, J. J.: Scaling of the Source Dimensions of Interface and Intraslab Subduction-zone Earthquakes with Moment Magnitude, Seismol. Res. Lett., 81, 941–950, doi:10.1785/gssrl.81.6.941, 2010.

Stucchi, M., Rovida, A., Gomez Capera, A. A., Alexandre, P., Camelbeeck, T., Demircioglu, M. B., Gasperini, P., Kouskouna, V., Musson, R. M. W., Radulian, M., Sesetyan, K., Vilanova, S., Baumont, D., Bungum, H., Fäh, D., Lenhardt, W., Makropoulos, K., Martinez Solares, J. M., Scotti, O., Živčić, M., Albini, P., Batllo, J., Papaioannou, C., Tatevossian, R., Locati, M.,

Meletti, C., Viganò, D., and Giardini, D.: The SHARE European Earthquake Catalogue (SHEEC) 1000–1899, J. Seismol., doi:10.1007/s10950-012-9335-2, online first, 2012.

Suckale, J., Rondenay, S., Sachpazi, M., Charalampakis, M., Hosa, A., and Royden, L. H.: High-resolution seismic imaging of the western Hellenic subduction zone using teleseismic scattered waves, Geophys. J. Int., 178, 775–791, doi:10.1111/j.1365-246X.2009.04170.x, 2009.

Synolakis, C. E.: Green's law and the evolution of solitary waves, Phys. Fluids A-Fluid, 3, 490–492, doi:10.1063/1.858107, 1991.

Tang, L., Titov, V. V., and Chamberlin, C. D.: Development, testing, and applications of site-specific tsunami inundation models for real-time forecasting, J. Geophys. Res., 114, C12025, doi:10.1029/2009JC005476, 2009.

Taymaz, T., Jackson, J., and Westaway, R.: Earthquake mechanisms in the Hellenic Trench near Crete, Geophys. J. Int., 102, 695–731, doi:10.1111/j.1365-246X.1990.tb04590.x, 1990.

Tiberti, M. M., Lorito, S., Basili, R., Kastelic, V., Piatanesi, A., and Valensise, G.: Scenarios of earthquake-generated tsunamis for the Italian coast of the Adriatic Sea, Pure Appl. Geophys., 165, 2117–2142, doi:10.1007/s00024-008-0417-6, 2008.

Tinti, S., Armigliato, A., and Bortolucci, E.: Contribution of tsunami data analysis to constrain the seismic source: the case of the 1693 eastern Sicily earthquake, J. Seismol., 5, 41-61, doi:10.1023/A:1009817601760, 2001.

Tinti, S. and Armigliato, A.: The use of scenarios to evaluate the tsunami impact in southern Italy, Mar. Geol., 199, 221–243, doi:10.1016/S0025-3227(03)00192-0, 2003.

Tinti, S., Zaniboni, F., Pagnoni, G., and Manucci, A.: Stromboli Island (Italy): Scenarios of tsunamis generated by submarine landslides, Pure Appl. Geophys., 165, 2143–2167, doi:10.1007/s00024-008-0420-y, 2008.

Torelli, L., Grasso, M., Mazzoldi, G., Peis, D., and Gori, D.: Cretaceous to Neogene structural evolution of the Lampedusa Shelf (Pelagian Sea, Central Mediterranean), Terra Nova, 7, 200–212, doi:10.1111/j.1365-3121.1995.tb00689.x, 1995.

van Der Meer, F. and Cloetingh, S.: Intraplate stresses and the subsidence history of the Sirte Basin (Libya), Tectonophysics, 226, 37–58, doi:10.1016/0040-1951(93)90109-W, 1993.

Van Dijk, J. P., Bello, M., Brancaleoni, G. P., Cantarella, G., Costa, V., Frixa, A., Golfetto, F., Merlini, S., Riva, M., Torricelli, S., Toscano, C., and Zerilli, A.: A regional structural model for the northern sector of the Calabrian Arc (southern Italy), Tectonophysics, 324, 267–320, doi:10.1016/s0040-1951(00)00139-6, 2000.

Vanneste, K., Camelbeeck, T., and Verbeeck, K.: A Model of Composite Seismic Sources for the Lower Rhine Graben, NW Europe, B. Seismol. Soc. Am., 103, 2, doi:10.1785/0120120037, 2013.

Vannucci, G., Pondrelli, S., Argnani, A., Morelli, A., Gasperini, P., and Boschi, E.: An Atlas of Mediterranean seismicity, Ann. Geophys.-Italy, 47-Supplement, 1, 247–306, 2004.

Velaj, T.: Evaporites in Albania and their impact on the thrusting processes, Balkan Geophys. Soc., 4, 9–18, 2001.

Visini, F., De Nardis, R., Barbano, M. S., and Lavecchia, G.: The highly debated seismogenic source of the 1693 eastern Sicily earthquake: some constrains from macroseismic field simulations, Rend. Online SGI, 1, 191–194, 2008.

Visini, F., De Nardis, R., Barbano, M. S., and Lavecchia, G.: Testing the seismogenic sources of the January 11th 1693 Sicilian earthquake (Io X/XI): insights from macroseismic field simulations, Ital. J. Geosci., 128, 147–156, 2009.

Yem, L. M., Camera, L., Mascle, J., and Ribodetti, A.: Seismic stratigraphy and deformational styles of the offshore Cyrenaica (Libya) and bordering Mediterranean Ridge, Geophys. J. Int., 185, 65–77, doi:10.1111/j.1365-246X.2011.04928.x, 2011.